Nano Research

Open Access

Research Article

# Curcumin-loaded multifunctional hydrogel drives spinal cord neural regeneration through immune microenvironment remodeling

Yiyang Hou[1], Yuxing Jiang[2], Xiaoyuan Niu[1], Yihan Li[1], Tao Zhu[2], Hongtao Rong[2]✉, Yu Yi[3]✉, and Lianyong Wang[1]✉

[1] College of Life Sciences, Key Laboratory of Bioactive Materials (Ministry of Education), Nankai University, Tianjin 300071, China
[2] Tianjin Medical University General Hospital, Tianjin 300052, China
[3] CAS Center for Excellence in Nanoscience, CAS Key Laboratory for Biomedical Effects of Nanomaterials and Nanosafety, National Center for Nanoscience and Technology, Beijing 100190, China

Cite this article: *Nano Research*, **2026**, *19*, 94908574. https://doi.org/10.26599/NR.2026.94908574

**ABSTRACT:** Spinal cord injury (SCI) is a severe central nervous system disorder that leads to long-term neurological dysfunction. Currently, there are no effective clinical treatments, making it imperative to develop novel therapeutic strategies that can simultaneously regulate immune responses and promote neural regeneration. Here, we designed and prepared an injectable self-healing multifunctional hydrogel composed of gelatin, quaternized chitosan, polydopamine, and curcumin. This hydrogel integrates immune microenvironment remodeling, spinal cord-matched mechanical properties, excellent biocompatibility, and sustained curcumin release for up to 14 days, effectively covering the critical acute-to-subacute phases of SCI repair. *In vitro* studies demonstrated that the hydrogel effectively scavenged reactive oxygen species (ROS) and induced macrophage polarization towards the anti-inflammatory M2 phenotype. In the rat model of SCI, treatment markedly alleviated oxidative stress and neuroinflammation during the acute phase, inhibited glial scar formation, promoted axonal and myelin regeneration, and ultimately improved motor function recovery. Collectively, this study presents a promising platform for SCI treatment and other central nervous system disorders by remodeling the immune microenvironment.

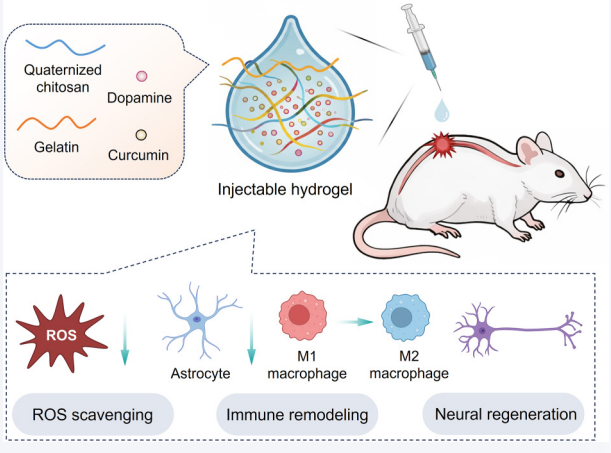


**KEYWORDS:** spinal cord repair, immunomodulatory hydrogel, mechanical matching, neuroinflammation modulation, neural regeneration

## 1 Introduction

Traumatic spinal cord injury (SCI), caused by external physical forces, is among the most devastating injuries to the central nervous system. It typically results in the loss of motor, sensory, and autonomic functions [1]. Each year, approximately 500,000 new cases of SCI are reported worldwide, imposing significant physical, emotional, and financial burdens on affected individuals and their families [2]. The poor prognosis of SCI is primarily attributed to the limited regenerative capacity of spinal cord tissue and the complex cascade of secondary injury processes, including inflammation, oxidative stress, and glial scar formation [3]. Currently, the standard clinical approach combines surgical decompression with high-dose glucocorticoid therapy. However, this treatment strategy is frequently associated with severe adverse effects, such as immunosuppression syndrome, which may exacerbate SCI and lead to systemic organ failure [4]. Therefore, it is urgent to develop more effective therapeutic strategies to promote functional recovery in patients with SCI.

SCI often triggers a cascade of secondary pathological events, including a pronounced inflammatory response and elevated oxidative stress [5]. The inflammatory process is driven by sustained macrophage activation and the release of pro-

**Received:** January 17, 2026; **Revised:** February 10, 2026
**Accepted:** February 13, 2026

✉Address correspondence to Hongtao Rong, hongtao.rong@tmu.edu.cn; Yu Yi, yiyu@nanoctr.cn; Lianyong Wang, wly@nankai.edu.cn

inflammatory mediators [6]. At the acute phase of injury, M1-type macrophages dominate the lesion site and produce excessive inflammatory cytokines and reactive oxygen species (ROS). These factors contribute to oxidative stress, exacerbate tissue damage, and promote apoptosis and necrosis of neurons and glial cells [7]. Moreover, the presence of ROS and inflammatory factors further recruits immune cells, such as neutrophils, to intensify tissue injury, leading to the formation of dense glial scars that physically and biochemically impede axonal regeneration, ultimately contributing to long-term neurological deficits and motor dysfunction [8, 9]. In contrast, M2-type macrophages exert neuroprotective effects by attenuating inflammation and supporting tissue repair and axonal growth [10]. Overall, effective therapeutic strategies for SCI should modulate the immune microenvironment, specifically suppress neurotoxic inflammation and oxidative stress, to promote neural regeneration and functional recovery after SCI.

In recent years, various strategies have been explored for treating SCI. Feng et al. promoted axonal growth and repaired SCI by modulating the mechanism of fibrous scar formation [11]. Liu et al. repaired SCI by releasing bioactive factors through a catheter to reduce oxidative stress [12]. Xiao et al. designed a nanocomposite hydrogel to enhance nerve regeneration for treating SCI [13]. We developed a biomimetic microneedle patch using macrophage membrane-coated nanoparticles to deliver brain-derived neurotrophic factor, which significantly enhanced targeted accumulation and neural repair in SCI [14]. Among them, regenerative medicine using biomaterials shows particular promise [15]. Hydrogels with three-dimensional structure have garnered significant attention due to their mechanical compatibility with spinal cord tissue and physicochemical properties that closely mimic the natural extracellular matrix [16]. Injectable hydrogels offer additional advantages, providing a supportive scaffold at irregular lesion sites for axonal growth and neural regeneration. For example, Nazemi et al. developed an injectable hydrogel incorporating the neuroregenerative drug paclitaxel for SCI repair [17]. Yang et al. designed a collagen-based hydrogel loaded with small molecules to restore motor function following SCI [18]. To enhance the durability of hydrogels under physiological conditions, the concept of self-healing has been introduced. Self-healing hydrogels can autonomously repair mechanical damage, maintaining structural integrity and functionality throughout the prolonged process of neural regeneration. Luo et al. prepared an injectable hydrogel using Fmoc-grafted chitosan and Fmoc peptides, which promoted neural repair by modulating local inflammation [19]. Similarly, Liu et al. developed a hyaluronic acid-chitosan self-healing hydrogel with a semi-interpenetrating polymer network, capable of facilitating central nervous system repair [20]. Despite these advancements, and the displayed considerable potential for SCI treatment, the development of the hydrogel with the function of effectively modulating the immune microenvironment of SCI is still desirable.

Based on the rationale mentioned above, we engineered an injectable, self-healing composite hydrogel, Gel-QCS-PDA-Cur (GQPC), for the treatment of SCI. This hydrogel integrates multiple biocompatible components with complementary functions. Gelatin (Gel), as a key constituent of the extracellular matrix (ECM) in the central nervous system, offers excellent biocompatibility and strong affinity for cells and tissue, thereby providing an ECM-mimicking microenvironment at the injury site [21]. Quaternized chitosan (QCS), a naturally derived polymer, supports neuronal adhesion and growth [22]. Polydopamine (PDA), enriched with amine, imine, and catechol groups, imparts strong adhesion and antioxidant properties to the hydrogel, enabling conformal coverage of irregular injury sites [23]. It has been reported to promote axonal growth and neuronal differentiation [24]. PDA further forms covalent Schiff base crosslinks with Gel and QCS, conferring self-healing, injectability, and enhanced mechanical strength. This self-healing capability enables conformal lesion coverage, structural resilience in dynamic environments, and stable, sustained drug delivery for reliable spinal cord repair. Curcumin (Cur), a natural polyphenol derived from *Curcuma longa* rhizomes, provides anti-inflammatory, antioxidant, and neuroprotective activities [25]. Its incorporation into the hydrogel overcomes intrinsic solubility and bioavailability limitations [26], and enables sustained local delivery to modulate the injury microenvironment.

Using this platform, we demonstrate that GQPC hydrogels promote neural repair following SCI. The hydrogel exhibited favorable mechanical properties, injectability, biocompatibility, and self-healing capability. Moreover, it enabled sustained curcumin release for up to 14 days, matching the critical therapeutic window spanning the acute to subacute phases of SCI. Both *in vitro* and *in vivo* results demonstrated that the hydrogel effectively remodeled the immune microenvironment through its anti-oxidative and anti-inflammatory effects, thereby attenuating glial scar formation, supporting neuronal regeneration, and significantly enhancing motor function recovery in SCI rats. Collectively, these findings highlight this hydrogel as a promising therapeutic strategy for SCI and provide a versatile platform for the treatment of central nervous system injuries.

## 2 Experimental

### 2.1 Materials

Quaternized chitosan (40% substitution) was bought from Macklin Biochemical Co., Ltd. (Shanghai, China). Gelatin, dopamine, curcumin, 2,2-diphenyl-1-picrylhydrazyl (DPPH), and 2,2'-azino-bis (3-ethylbenzothiazoline-6-sulfonic acid) (ABTS) were purchased from Aladdin Biochemical Technology Co., Ltd. (Shanghai, China). Rat adrenal medullary chromaffin tumor cells (PC12), human neuroblastoma cells (SH-SY5Y), and mouse monocyte macrophage leukemia cells (RAW264.7) were from Fuhang Biotechnology Co., Ltd. (Shanghai, China). Calcein-AM/PI Cell Viability, Cell Counting Kit-8 (CCK-8), tumor necrosis factor-$\alpha$ (TNF-$\alpha$), interleukin-1$\beta$ (IL-1$\beta$), and interleukin-10 (IL-10) enzyme-linked immunosorbent assay (ELISA) kits, lipopolysaccharide (LPS), and recombinant mouse interferon-$\gamma$ (IFN-$\gamma$) were obtained from Solarbio Science & Technology Co., Ltd. (Beijing, China). Dulbecco's modified Eagle medium (DMEM), trypsin, fetal bovine serum (FBS), Penicillin, and Streptomycin antibiotic mixture were supplied from Thermo Fisher Biochemical Product Co., Ltd. (Beijing, China). NF200, CD86, and CD206 were bought from Signalway Biotechnology Co., Ltd. (Nanjing, China). Glial fibrillary acidic protein (GFAP) and neuronal nuclei (NEUN) were from Abcam (Shanghai, China). 4',6-diamidino-2-phenylindole (DAPI) was purchased from Sigma-Aldrich Corporation (USA). All chemicals were of analytical grade and could be used without further purification.

## 2.2 Synthesis of hydrogels

QCS was dissolved in deionized water and stirred overnight using a magnetic stirrer to obtain the 4 wt.% QCS solution. The Gel was dissolved in deionized water at 60 °C for 4 h to obtain a 20 wt.% Gel solution. The Gel-QCS solution was prepared by mixing equal volumes of Gel (20 wt.%) and QCS (4 wt.%). A certain amount of $NaIO_4$ and DA was sequentially added to the Gel-QCS solution, in which the concentrations of $NaIO_4$ and DA were fixed at 0.5 wt.% and 1 wt.%, respectively. Cur was then dissolved in anhydrous ethanol to prepare a stock solution at 200 mg/mL. Under vortex mixing, different volumes of the Cur stock solution were added dropwise into the GQP solution, and vortexing was continued until a homogeneous precursor solution was formed. Finally, Gel-QCS-PDA-Cur1.5, Gel-QCS-PDA-Cur3, Gel-QCS-PDA-Cur4.5, and Gel-QCS-PDA-Cur6 hydrogels with the Cur contents of 1.5 wt.%, 3 wt.%, 4.5 wt.%, and 6 wt.% (defined as the mass fraction relative to the final hydrogel precursor solution), respectively. These were designated as GQPC1.5, GQPC3, GQPC4.5, and GQPC6. The prepared hydrogels were stored at room temperature for subsequent experiments.

## 2.3 Characterization of hydrogels

### *2.3.1 Fourier transform infrared spectrometer (FT-IR) and scanning electron microscope (SEM)*

The Gel-QCS, GQP, GQPC1.5, GQPC3, GQPC4.5, and GQPC6 hydrogels were lyophilized by a freeze dryer (SCIENTZ-10 ND, China). The FT-IR spectra of hydrogels were obtained using an FT-IR spectrometer (Bruker TENSOR II, Germany), scanned over 4000–400 $cm^{-1}$. The microscopic morphology was observed using SEM (Apreo S LoVac, Czech Republic) after platinum coating of the cross-sections of the samples.

### *2.3.2 Swelling property of hydrogels*

The freeze-dried GQP, GQPC1.5, GQPC3, GQPC4.5, and GQPC6 hydrogels were weighed as the initial mass $M_0$ and then soaked in phosphate-buffered saline (PBS) at 37 °C. After the freeze-dried hydrogels were fully swollen (approximately 46–48 h), the excess liquid on the surface was gently absorbed with filter paper. The swelling hydrogel was then weighed as $M_1$. The swelling ratio of the hydrogels was calculated according to the equation (Eq. (1)):

$$\text{Swelling ratio}\ (\%) = M_1/M_0 \times 100\% \quad (1)$$

### *2.3.3 In vitro degradation of hydrogels*

The *in vitro* degradation of hydrogels was determined via the experimental method described by Su et al. [27] with appropriate modifications. The freeze-dried GQP, GQPC1.5, GQPC3, GQPC4.5, and GQPC6 hydrogels were weighed and recorded as $M_0$. Then, the pre-weighed hydrogels were immersed in PBS solution containing type II collagenase (2 U/mL) and incubated at 37 °C. The remaining mass of the hydrogels at different time points was weighed as $M_1$. The degradation rate of the hydrogels was calculated according to equation (Eq. (2)):

$$\text{Mass remaining}\ (\%) = (M_0 - M_1)/M_0 \times 100\% \quad (2)$$

### *2.3.4 Mechanical properties of hydrogels*

Rectangular sheet hydrogel samples with dimensions of 40 mm × 8 mm × 3 mm were prepared. The tensile properties of the hydrogel samples were evaluated using a universal testing machine (Instron 5960) at a tensile rate of 10 mm/min. Cylindrical hydrogels with a diameter of 15 mm and a height of 10 mm were prepared. The uniaxial compression and cyclic compression properties of samples were tested using a universal testing machine at a compression rate of 10 mm/min, with a 50% compression strain and 10 cycles of cyclic compression.

### *2.3.5 Rheological behaviors of hydrogel*

The rheological behavior of the hydrogels was tested using a rheometer (TA Discovery 170 HR-2, USA), and the storage modulus ($G'$) and loss modulus ($G''$) were recorded. The hydrogels were placed on the lower plate of the rheometer at 37 °C using a 20 mm parallel plate fixture with a 1 mm gap between the parallel plate measurement cells. The linear viscoelasticity was tested at a fixed angular frequency of 10 rad/s. The low (1%)–high (1500%)–low (1%) step strain rheology experiments were performed at a fixed angular frequency (10 rad/s). The shear viscosity was measured at shear rates from 0.1 to 100 $s^{-1}$. The dynamic frequency scans were performed at a fixed strain of 1% and over a frequency range of 0.01 to 10 rad/s. During the experiments, a ring of low-viscosity silicone oil was dripped around the hydrogel sample on the lower plate of the rheometer to prevent water evaporation.

### *2.3.6 The release profile of Cur*

The release profile of Cur from the hydrogels was determined according to the method described by Luo et al. [19]. A standard curve for Cur was first constructed by recording the absorbance at 429 nm of a series of Cur solutions with concentrations (0.9375, 1.875, 3.75, 7.5, 15, and 30 μg/mL). The 500 μL GQPC hydrogel was placed into 1 mL of saline solution and incubated at 37 °C with shaking at 100 rpm. At a preplanned time point, the released concentration of Cur was determined using an ultraviolet–visible (UV–Vis) spectrophotometer (Shimadzu). The release profile of Cur was plotted.

### *2.3.7 In vitro antioxidant property of hydrogel*

The antioxidant properties of the hydrogel were investigated by measuring its capacity to scavenge DPPH, ABTS, hydrogen peroxide ($H_2O_2$), superoxide ($\cdot O_2^-$), and the hydroxyl radical (·OH). For DPPH measurement, 200 μL of hydrogel was immersed in 1 mL of 0.1 mM DPPH in methanol and incubated at 37 °C for 30 min in the dark. The DPPH scavenging was determined by measuring the absorbance of the solution at 517 nm. An equal volume of deionized water replaced the hydrogel samples as the control group.

For ABTS measurement, 7.4 mM ABTS was mixed with a 2.4 mM potassium persulfate solution in equal volume. Then, 200 μL of hydrogel was mixed with the ABTS solution and incubated at 37 °C in the dark for 30 min. The absorbance was measured at 730 nm to determine the ABTS scavenging. Potassium persulfate solution was used as the control.

The $H_2O_2$, $\cdot O_2^-$, and ·OH were determined using the $H_2O_2$ content assay kit (BC3595, Solabio), the $\cdot O_2^-$ assay kit (Nanjing Jiancheng Bioengineering Institute), and the ·OH scavenging capacity assay kit (BC1320, Solabio), respectively.

### 2.4 *In vitro* biological evaluation of hydrogel

#### 2.4.1 *Cytotoxicity of hydrogel*

We evaluated the cytotoxicity of the hydrogel using the leaching method [28]. The GQPC hydrogels were first washed and sterilized with 75% (v/v) ethanol, then irradiated with UV light for 1 h. The sterilized GQPC hydrogel was soaked in DMEM to obtain hydrogel leachate, which was then diluted to various concentrations for further use.

The PC12 cells were seeded into 96-well plates at a density of $5 \times 10^3$ cells/well and incubated for 24 h to ensure cell adhesion. Then the culture medium was discarded, and the above hydrogel leachate of different concentrations was added. After the cells and hydrogel leachate were co-cultured for 24 h at 37 °C in an incubator containing 5% $CO_2$, 10 μL of CCK-8 solution was added to each well, and the absorbance at 450 nm was measured via an enzyme meter to evaluate the cytotoxicity of GQPC hydrogel.

#### 2.4.2 *Live/dead staining of cells*

We assessed the effect of the hydrogel on cell viability using live/dead staining. When PC12 cells reached a stable state, hydrogel leachate was added, and the cells were co-cultured for 24 and 48 h. The cells were then stained with calcein and propidium iodide, respectively. Finally, cell viability was assessed by live/dead staining using a laser confocal microscope (NIKON, Japan), and fluorescence intensity was analyzed using ImageJ software.

#### 2.4.3 *Hemolysis assay*

We evaluated the blood compatibility of the GQPC hydrogel using a hemolysis assay. Whole blood from mice was collected with sodium citrate as an anticoagulant, then centrifuged at 3000 rpm for 15 min to obtain a red cell suspension. Then, 20 μL of the red cell suspension was mixed with 1 mL of leachate at different concentrations in centrifuge tubes. $H_2O$ and PBS were used as positive and negative controls, respectively. After incubation at 37 °C for 4 h and centrifugation at 3000 rpm for 15 min, the centrifuge tubes were aligned to the same level and photographed. Finally, the supernatant was transferred to a 96-well plate, and absorbance was measured at 542 nm using an enzyme meter to assess hemolysis.

#### 2.4.4 *Antioxidant capacity testing under oxidative stress of cells*

The antioxidant capacity of the hydrogel was first investigated by assessing the downregulation of intracellular ROS levels in RAW264.7 cells under oxidative stress [29]. RAW264.7 cells were seeded in confocal dishes at a density of $3 \times 10^5$ cells/mL and incubated at 37 °C with 5% $CO_2$ for 24 h, then 1 mL of 10 μM of the fluorescent probe 2',7'-dichlorofluorescein diacetate (DCFH-DA) in serum-free medium was added and co-incubated at 37 °C in the dark for 30 min. Subsequently, DCFH-DA was removed, and the cells were washed with serum-free medium. 200 μM $H_2O_2$ was added to stimulate the cells containing DCFH-DA for 24 h, and then washed with serum-free medium to obtain cells with oxidative free radicals (as the positive control group). The hydrogel leachates were co-incubated with cells exposed to oxidative free radicals (as the experimental group), and cells not stimulated with $H_2O_2$ were used as the negative control group. Finally, the cells were observed by confocal laser microscopy, and fluorescence intensity was analyzed using ImageJ software.

The inhibitory effect of the hydrogel on oxidative apoptosis in SH-SY5Y cells was investigated according to the methods of Wan et al. [30], with appropriate modifications. The SH-SY5Y cells were seeded at $1 \times 10^4$ cells/well in 96-well plates and incubated for 24 h. Then, the SH-SY5Y cells were treated with different concentrations of $H_2O_2$, and cell viability was assessed using the CCK-8 kit. Based on CCK-8 results, the optimal $H_2O_2$ concentration was selected to stimulate SH-SY5Y cells, which were subsequently treated with hydrogel leachates from different hydrogels for 24 h, and cell viability was measured using the CCK-8 kit (Solarbio, China).

#### 2.4.5 *In vitro assessment of macrophage polarization*

The RAW264.7 cells were cultured in DMEM medium containing 10% FBS, and passaged into confocal dishes when cell density reached 70%–80%. Then the RAW264.7 cells were rinsed with PBS and sequentially fixed with 4% paraformaldehyde, permeabilized with 0.2% TritonX-100, and blocked with 1% bovine serum albumin (BSA) solution. The cells were incubated overnight at 4 °C with CD86 primary antibody (1:100 dilution, 48763, SAB) and CD206 primary antibody (1:200 dilution, 49238, SAB). Then, CD86 secondary antibody (1:500 dilution, L35451, SAB) and CD206 secondary antibody (1:500 dilution, L35190, SAB) were incubated with the cells at room temperature for 1 h, after which the cells were restained with DAPI. Finally, the cells were observed under a laser confocal microscope, and the images were analyzed using ImageJ software.

The RAW264.7 cells were stimulated with 20 ng/mL IFN-$\gamma$ and 100 ng/mL LPS for 24 h. The cell supernatants were collected after co-culturing with hydrogel leachates, and the concentrations of TNF-$\alpha$, IL-1$\beta$, and IL-10 were quantified using ELISA kits.

### 2.5 Animal experiment

#### 2.5.1 *Construction and treatment of the SCI model*

The procedures of animal experiment were approved by the Animal Ethics Committee of Nankai University (Approval No. 2024-SYDWLL-000642) and complied with the guidelines of the National Research Council for the care and use of laboratory animals. Female Sprague-Dawley rats (6–8 weeks, 200–220 g) were purchased from Beijing Vital River Laboratory Animal Technology Co., Ltd. For the construction of the SCI model, the SD rats were anesthetized via intraperitoneal injection of 2% pentobarbital sodium (30 mg/kg body weight). After anesthesia, the rats were placed in a prone position, and their backs were shaved and sterilized with iodophor. The skin was then incised along the T9–T10 intervertebral space (approximately 2 cm) to expose the spinal cord of the T9 segment. The weight-drop spinal cord impactor system (MEYUE Biotechnology Co., Ltd.) was employed to cause contusive SCI (a cylindrical flat head hammer of 2.5 mm in diameter, a rod of 20 g in weight and 20 mm in height, and a dwell time of 5 s). Criteria for successful construction of the SCI model were the presence of contusion at the site of injury, spastic swaying of the tail, and twitching of both hind limbs. For the treatment of SCI, oozing blood on the dorsal surface of the injured spinal cord was absorbed using a sterile cotton swab. The SD rats with SCI were randomly divided into four groups (10 rats in each group), including the control group (sham-operated group), the saline group (treated with saline after SCI), the GQP group (treated with GQP hydrogel after SCI), and the GQPC group (treated with GQPC hydrogel after SCI). After 10 μL of saline or hydrogel was

injected into the lesion site of SCI, the muscle tissue and skin were sequentially sutured. During the first 3 days after SCI, gentamicin was injected into the leg muscles of SCI rats once a day at a dose of 8 mg/kg. Meanwhile, the bladders of the rats were manually squeezed every 12 h until urinary function was restored.

#### 2.5.2 *Evaluation of motor function recovery of SCI rats*

We used the Basso-Beattie-Bresnahan (BBB) motor rating scale, gait analysis, inclined plane test, and grid-walking test to evaluate hindlimb motor function recovery after SCI in rats. Three independent assessors performed all evaluations. BBB scores ranged from 0 (complete paralysis without hindlimb locomotion) to 21 (normal locomotion, coordinated gait, and parallel placement of both paws). The rats were placed in an open field and allowed to move freely for 5 min before the assessment, and the BBB scores were assessed at days 1, 3, 7, 14, 21, and 28 post-injury. For footprint analysis, the rat's forelimbs and hindlimbs were immersed in blue and red ink, respectively, and then restrained from walking straight on a piece of white paper. For the inclined plane experiment, all rats were placed on a wooden inclined plane, which was raised 5° at a time from the side of the rat's head. The maximum angle at which the rats maintained balance for 5 s on the inclined plane without falling was recorded. Additionally, the number of times the rat's hind paws touched the grid when its forelimbs moved on the flat grid for 100 steps was recorded.

#### 2.5.3 *Histologic staining and evaluation*

After 28 days, the treated SCI rats were executed by cardiac perfusion with PBS and 4% paraformaldehyde under anesthesia. The injured spinal cord was collected, embedded in paraffin, and sectioned (longitudinal sections of 3 μm thickness). To assess the morphological structure and myelin regeneration of the spinal cord, the tissue sections were stained with hematoxylin and eosin (H&E) and Luxol fast blue (LFB) and observed using a tissue section digital scanner (3DHISTECH, China).

#### 2.5.4 *Immunofluorescence staining and evaluation*

Paraffin-embedded sections of spinal cord were deparaffinized, rehydrated, and then subjected to antigen retrieval. The sections were rinsed with PBS (3×, 10 min), permeabilized with 0.1% Triton X-100, blocked with 3% BSA, and incubated overnight at 4 °C with the following primary antibodies: the CD86 primary antibody (1:100 dilution, 48763, SAB), the CD206 primary antibody (1:200 dilution, 49238, SAB), the NF200 (1:100 dilution C48259, SAB), NEUN (1:200 dilution, ab177487, Abcam), and GFAP (1:5000 dilution, ab7260, Abcam). After rinsing the sections with PBS (3×, 10 min ), the cells were incubated with Alexa Fluor staining coupled with species-appropriate secondary antibodies at room temperature for 1 h. After rinsing the sections with PBS (three times, 10 min each), the cells were restained with DAPI. Finally, the samples were observed under a laser confocal microscope, and the images were analyzed using ImageJ software.

#### 2.5.5 *Detection of inflammatory factors and neuronal antioxidant stress enzymes expression in spinal cord tissue after SCI*

Spinal cord tissues from different groups were collected on day 7 after injury and immediately homogenized in 1 mL PBS. After homogenization, the tissue was centrifuged at 3000*g* for 10 min, and the supernatant was collected for quantification of TNF-α, IL-1β, and IL-10 using the ELISA kit. The levels of superoxide dismutase (SOD), malondialdehyde (MDA), and glutathione peroxidase (GSH-Px) in the supernatants were also quantified using commercial assay kits (Beyotime, China).

### 2.6 Statistical analysis

The data are presented as mean ± standard deviation (mean ± SD). All statistical analyses were performed based on independent biological replicates. Multiple measurements obtained from the same biological sample (e.g., multiple imaging fields or repeated evaluations) were considered technical replicates and were not treated as independent data points. Statistical differences were analyzed using Student's t-test, one-way ANOVA ($n \geq 3$), or Tukey's post hoc test. The $P$ values less than 0.05 were considered statistically significant ($^{*}P < 0.05$, $^{**}P < 0.01$, and $^{***}P < 0.001$). Non-significant differences are denoted as n.s.

## 3 Results and discussion

### 3.1 Synthesis and characterization of hydrogels

Chitosan (CS) is an amino group-rich natural polysaccharide that is non-toxic and biodegradable [31]. But its insolubility under physiological conditions limits its applications. Among the derivatives of CS, QCS has attracted widespread attention due to its excellent solubility and antibacterial activity [32]. The Gel exhibits excellent biocompatibility and water solubility [33], and the mixture of Gel and QCS can form a hydrogel by electrostatic interactions between the carboxyl groups in the Gel and the quaternary ammonium groups in the QCS, along with hydrogen bonding. However, the rapid degradation and insufficient mechanical properties of Gel-QCS hydrogel are drawbacks. Based on this, we further introduced DA into the mixture of Gel and QCS. The free amino groups on the QCS backbone facilitate crosslinking between DA and QCS, forming a more stable hydrogel than the Gel-QCS hydrogel. To improve the mechanical properties and enhance antioxidant and anti-inflammatory properties of the hydrogel, Cur was added to prepare GQPC hydrogels. As shown in Scheme 1, the $NaIO_4$ could oxidize DA to dopaquinone and PDA with *o*-quinoid units. The PDA would covalently crosslink with QCS and Gel via Schiff base reaction between the amino groups and *o*-quinoid units to form a hydrogel (Fig. 1(a)).

All hydrogels exhibited uniform and interconnected porous networks (Fig. 1(b)), which are favorable for supporting neural cell extension and facilitating the exchange of nutrients and metabolic waste. FT-IR of the hydrogel was performed (Fig. 1(c)). The FT-IR spectrum of Gel displayed characteristic absorption peaks of amide I at 1630 $cm^{-1}$ and amide II at 1539 $cm^{-1}$ from N-H in-plane bending coupled with C–N stretching vibrations. The FT-IR spectrum of QCS revealed key peaks at 3293 $cm^{-1}$ (N–H stretching), 1477 $cm^{-1}$ (–$CH_3$ stretching), and 1022 $cm^{-1}$ (C-O-C stretching), consistent with its chemical structure of QCS [34]. For PDA, characteristic peaks were observed at 1616 $cm^{-1}$ (C=C stretching), 1498 $cm^{-1}$ (aromatic C–H bending), and 1285 $cm^{-1}$ (C–O stretching). Cur showed a broad O–H stretching vibration at 3500 $cm^{-1}$, a C=O stretching peak at 1626 $cm^{-1}$, and a C–O stretching peak associated with phenolic hydroxyl and methoxy groups at 1151 $cm^{-1}$. In the Gel-QCS composite, the intensity of the amide II band was reduced, suggesting hydrogen bonding and electrostatic interactions between the amino groups of Gel and the quaternary ammonium groups of QCS, which suppressed N–H

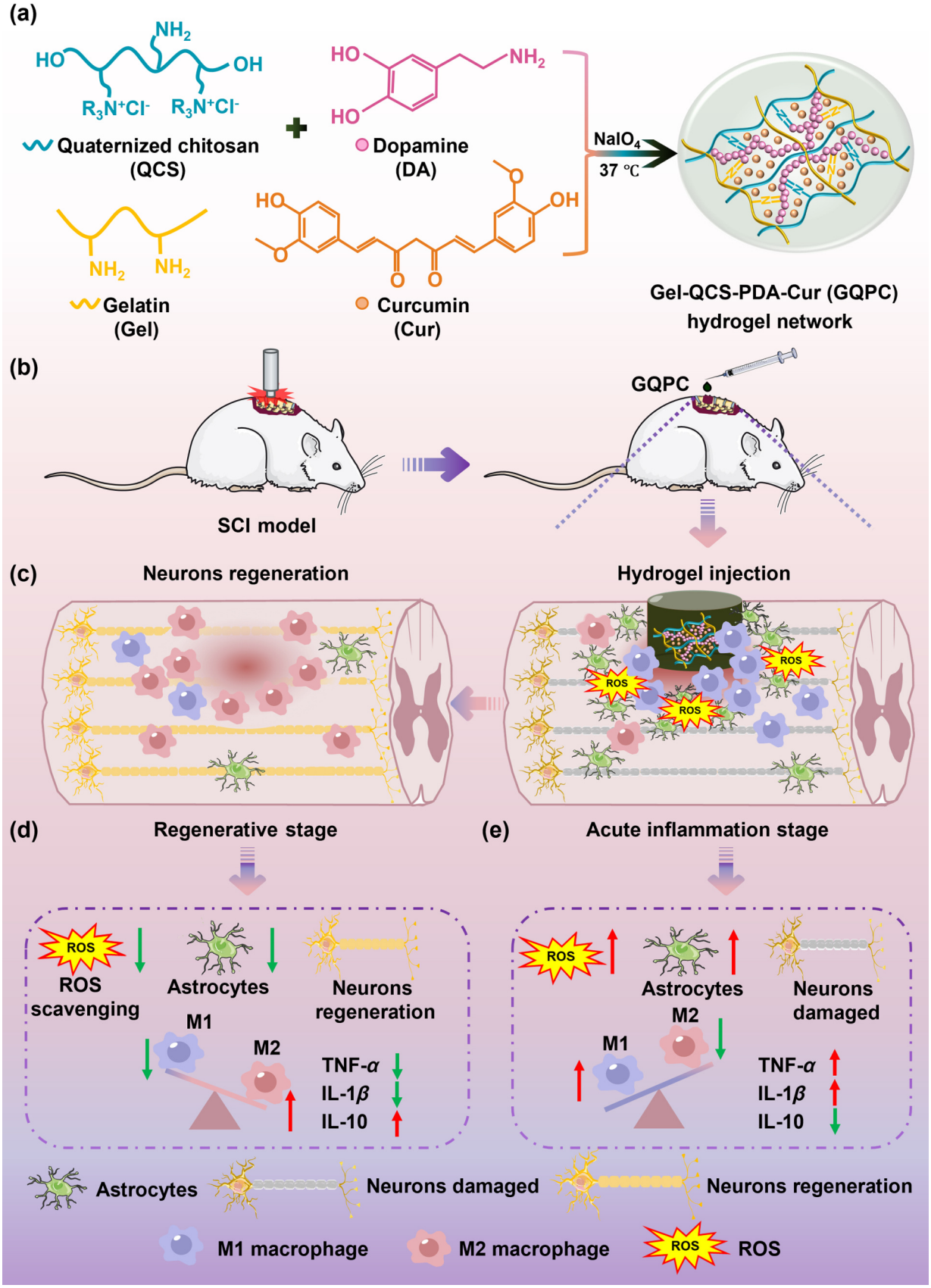


**Scheme 1** Schematic illustration of GQPC for neural regeneration. (a) Preparation of GQPC hydrogel. (b) Construction of the SCI model and hydrogel injection. (c) GQPC hydrogel achieves neural regeneration by remodeling the immune microenvironment to inhibit glial scar formation. (d) ROS and the immune microenvironment at the regenerative stage. (e) ROS and the immune microenvironment at the acute inflammation stage.

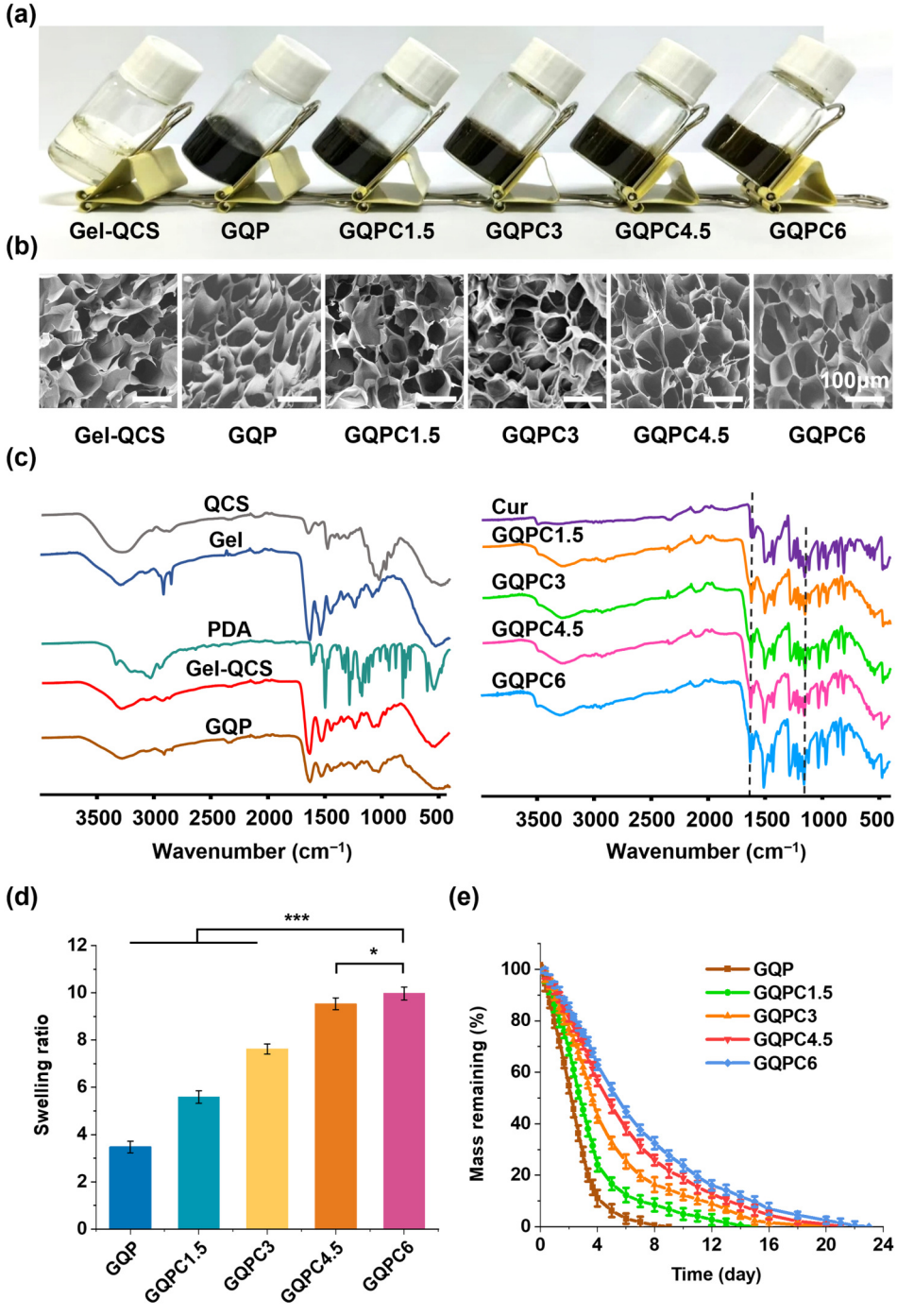


**Figure 1** Characterization of hydrogels. (a) Photographs of hydrogels prepared at room temperature. (b) SEM images of hydrogels. (c) FT-IR spectra of QCS, Gel, PDA, Cur, Gel-QCS, GQP, GQPC1.5, GQPC3, GQPC4.5, and GQPC6 in the range of 4000–400 $cm^{-1}$. (d) Swelling ratio of hydrogels. Data are presented as mean ± SD ($n$ = 3). *$P$ < 0.05 and ***$P$ < 0.001. (e) Degradation rates of hydrogels.

bending vibrations. The GQP hydrogel exhibited a broadened peak at 3293 $cm^{-1}$, attributed to the overlapping of intra- and intermolecular hydrogen bonds. This broadening, along with a weakened amide I band, suggested the formation of Schiff base bonds (C=N) [35, 36]. Finally, the FT-IR spectrum of GQPC retained characteristic peaks of Cur, and the intensity of the C=O stretching peak at 1626 $cm^{-1}$ and the C–O stretching peak at 1151 $cm^{-1}$ increased proportionally with the increase of Cur content, confirming the successful incorporation of Cur into the hydrogel matrix.

### 3.2 Swelling and degradation properties of hydrogels

In SCI treatment, hydrogels provide sustained structural support at the injury site and reduce the risk of secondary tissue damage [27], so a low swelling ratio and extended degradation time are desirable. As shown in Fig. 1(d), all hydrogel formulations maintained a swelling ratio of less than 10%, and the swelling ratio of the hydrogels increased slightly with the increase of Cur content, which can be attributed to the interfering effect of Cur on interchain hydrogen bonding within the hydrogel network [37]. Consequently,

the degree of crosslinking of the hydrogel network has been reduced, increasing the swelling ratio. The low swelling ratio will minimize the risk of mechanical compression of surrounding tissues following hydrogel injection. This is also beneficial for avoiding ischemia and further neuronal injury at the SCI site. Figure 1(e) presented the degradation profiles of hydrogels, all of which exhibited complete degradation within approximately 21 days. This degradation timeframe aligns well with the endogenous repair window of SCI, allowing the hydrogel to provide functional support throughout the critical phases of neural regeneration. The degradation behavior of Gel-QCS was not performed due to the rapid disintegration of the lyophilized Gel-QCS. This rapid disintegration could be attributed to the significantly weakened hydrogen bonding interactions within Gel-QCS [38], so the degradation behavior of Gel-QCS cannot be assessed accurately.

### 3.3 Antioxidant capacity of hydrogels

Excessive ROS accumulation further leads to oxidative damage, including lipid peroxidation, protein denaturation, and DNA fragmentation, all of which contribute to secondary neuronal death and hinder neural regeneration [39]. The hydrogels with intrinsic antioxidant properties can mitigate this damage by scavenging ROS and thereby alleviating oxidative stress. To evaluate the antioxidant capacity of the hydrogels *in vitro*, we performed a series of free radical scavenging assays, including DPPH, ABTS, $\cdot O_2^-$, ·OH, and $H_2O_2$ assays. As shown in Figs. 2(a)–2(e), the incorporation of PDA into the Gel-QCS matrix conferred a significant antioxidant effect, and the addition of Cur further enhanced this effect. The improved antioxidant performance is attributed to the phenolic hydroxyl groups present in both PDA and Cur, which can effectively scavenge free radicals. Among the hydrogels, GQPC4.5 and GQPC6 exhibited the highest antioxidant capacity, with no statistically significant difference. This plateau effect is likely due to the saturation of available Cur binding sites at 4.5 wt.%, so the increase of the concentration from 4.5 wt.% to 6 wt.% does not further enhance radical scavenging.

### 3.4 Mechanical properties of hydrogels

The mechanical compatibility between hydrogels and native spinal cord tissue is a critical factor influencing the success of SCI repair [40]. To assess this, we evaluated the mechanical properties of the hydrogels using both tensile and compression tests. As shown in Fig. 3(a), the tensile stress-strain curves revealed that the elasticity of the hydrogels increased with increasing Cur content, with GQPC6 exhibiting the highest elasticity. This Cur concentration-dependent enhancement suggests that Cur improves network integrity and flexibility. The natural spinal cord typically withstands compressive stresses of approximately 10 kPa [41]. As shown in Fig. 3(b), the compressive stress of all Cur-loaded hydrogels was within this physiological range, indicating good mechanical compatibility with spinal cord tissue. Moreover, the compressive resistance of the hydrogels increased with increasing Cur content. This was due to the formation of hydrogen bonds between the phenolic hydroxyl group and amino and hydroxyl groups as Cur concentration increased, leading to more crosslinking points within the hydrogel, thereby enhancing its mechanical properties.

Based on the antioxidant activity and mechanical compatibility, GQPC4.5 was selected as the optimal formulation for preparing the hydrogel (GQPC) for subsequent experiments. The fatigue resistance of the GQPC hydrogel was assessed through ten consecutive loading-unloading cycles at 50% deformation without intervals. As illustrated in Fig. 3(c), the hysteresis loops of the hydrogel nearly overlapped across cycles, and the area enclosed by the hysteresis curves remained consistent. These results indicated that the hydrogel exhibited excellent fatigue resistance, maintaining its mechanical integrity under repeated deformation. This is attributed to the formation of dynamic Schiff base bonds between PDA and the amino groups of Gel and QCS. These reversible covalent bonds contribute to efficient energy dissipation under mechanical stress, imparting the hydrogel with stability.

### 3.5 Rheological and drug release properties of hydrogel

The rheological behavior of GQPC hydrogel was assessed by measuring the storage modulus ($G'$) and loss modulus ($G''$). As shown in Fig. 3(d), the gelation remained intact until the applied strain exceeded 1063.69%, indicating that the hydrogel maintains a robust structure against high strain. Similarly, the dynamic frequency scanning test (Fig. 3(e)) revealed that the GQPC hydrogel exhibited weak frequency dependence. This indicated that the hydrogel possessed a stable network structure capable of maintaining mechanical integrity even under dynamic conditions, making it beneficial for SCI treatment. The step-strain experiment (Fig. 3(f)) demonstrated that the mechanical properties of GQPC hydrogel recovered rapidly and repeatedly when the strain was cyclically imposed between high and low strain, which was consistent with the mechanical cycling results (Fig. 3(c)), and confirmed its excellent self-healing ability and fatigue resistance. The self-healing ability, which was further visually confirmed in Figs. S1(a) and S1(b) in the Electronic Supplementary Material (ESM), was attributed primarily to the dynamic and reversible Schiff base bonds within the hydrogel network. We found that the hydrogel exhibited shear-thinning behavior, as shown in Fig. 3(g): the shear viscosity decreased with increasing shear rate. The shear-thinning behavior endows the hydrogel with injectable properties. Furthermore, Fig. 3(h) showed that Cur could sustain release over 14 days. This sustained release of Cur covered the acute-to-subacute repair phases of SCI, ensuring prolonged therapeutic activity.

### 3.6 Evaluation of *in vitro* biocompatibility and *in vitro* antioxidant capacity of hydrogel

We evaluated the *in vitro* biocompatibility of the GQPC hydrogel by measuring cytotoxicity using the CCK-8 assay and hemolysis. As shown in Fig. 4(a), PC12 cell viability remained above 95% after co-incubation with varying hydrogel leachate concentrations, indicating that the hydrogel possessed excellent cytocompatibility. The hemolysis assays demonstrated that the hemolysis rates across all tested concentrations were below 5% (Fig. 4(b)), confirming the favorable blood compatibility of the GQPC hydrogel. Furthermore, live/dead staining (Fig. 4(c)) revealed that the hydrogel had no significant cytotoxic effects on PC12 cells after 24 and 48 h of culture with hydrogel leachate, as supported by cell viability (Fig. 4(d)). Together, these results confirmed that the GQPC hydrogel was highly biocompatible, making it suitable for *in vivo* applications.

Following SCI, excessive ROS production leads to elevated oxidative stress, which can exacerbate inflammation, promote cell apoptosis, and contribute to secondary tissue damage [42]. To mimic the oxidative stress environment after SCI, $H_2O_2$ was used to stimulate RAW264.7 cells, and intracellular ROS levels were

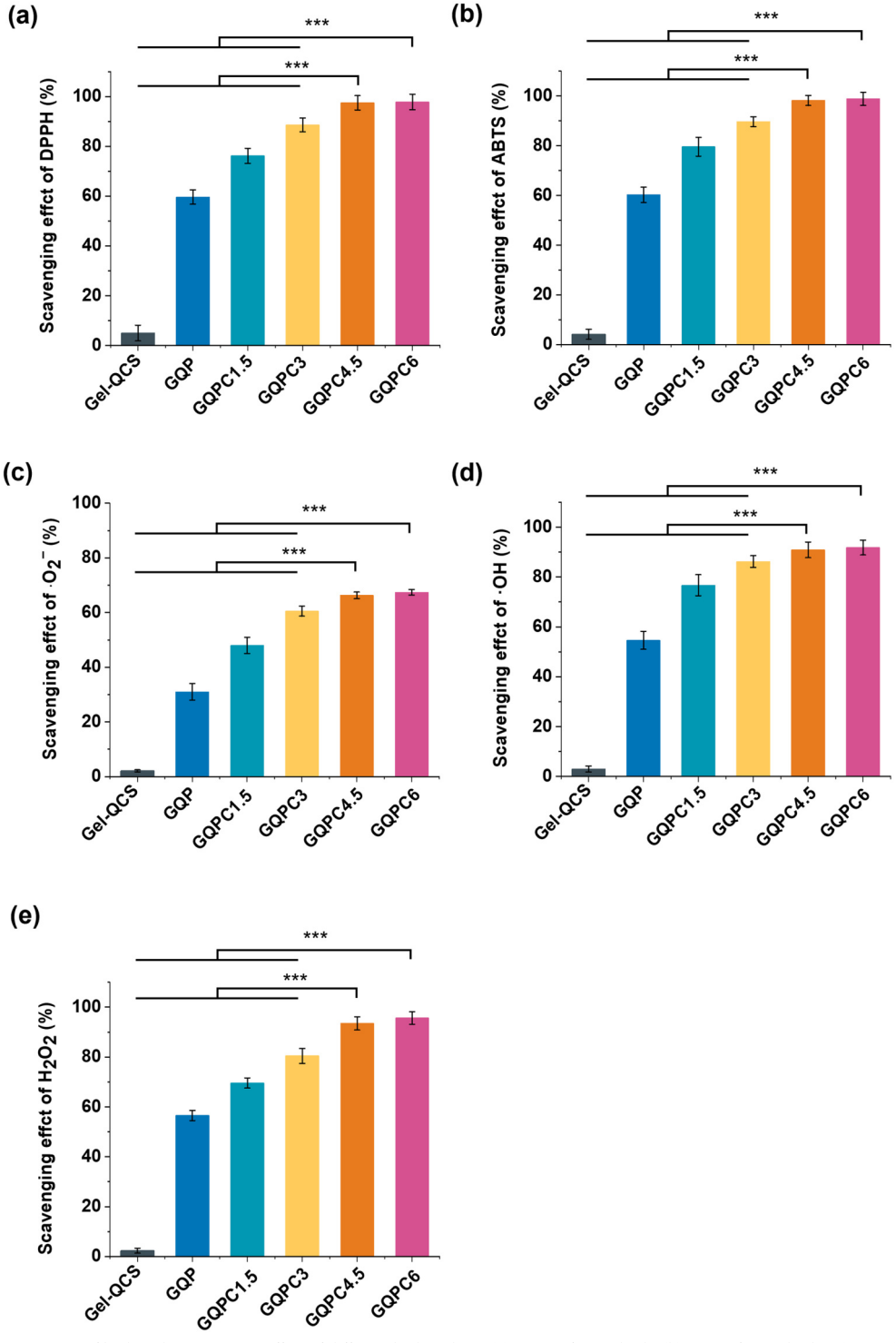


**Figure 2** Antioxidant properties of hydrogels. Scavenging effect of different hydrogels on (a) DPPH free radicals, (b) ABTS free radicals, (c) $\cdot O_2^-$, (d) ·OH, and (e) $H_2O_2$. Data are represented as mean ± SD ($n = 3$) in panels (a)–(e). ***$P < 0.001$.

measured using DCFH-DA fluorescence staining. As shown in Fig. 5(a), the intensity of green fluorescence significantly increased after $H_2O_2$ treatment, indicating intracellular ROS levels rose. The green fluorescence intensity significantly reduced after treatment with GQP and GQPC hydrogels. The cells treated with GQPC hydrogel exhibited the lowest green fluorescence intensity, which was not significantly different from the negative control group (Fig. 5(b)). This result confirmed that the GQPC hydrogel effectively scavenged intracellular ROS, which was attributed to the synergistic antioxidant effects of PDA and Cur. The superior antioxidant capacity of GQPC hydrogel enables it to protect cells from oxidative stress-induced damage and to contribute to the repair process following SCI.

By exposing SH-SY5Y cells to $H_2O_2$, we further evaluated the neuroprotective effects of GQPC hydrogel. The concentration of $H_2O_2$ was optimized as 400 μM, resulting in a cell survival rate of

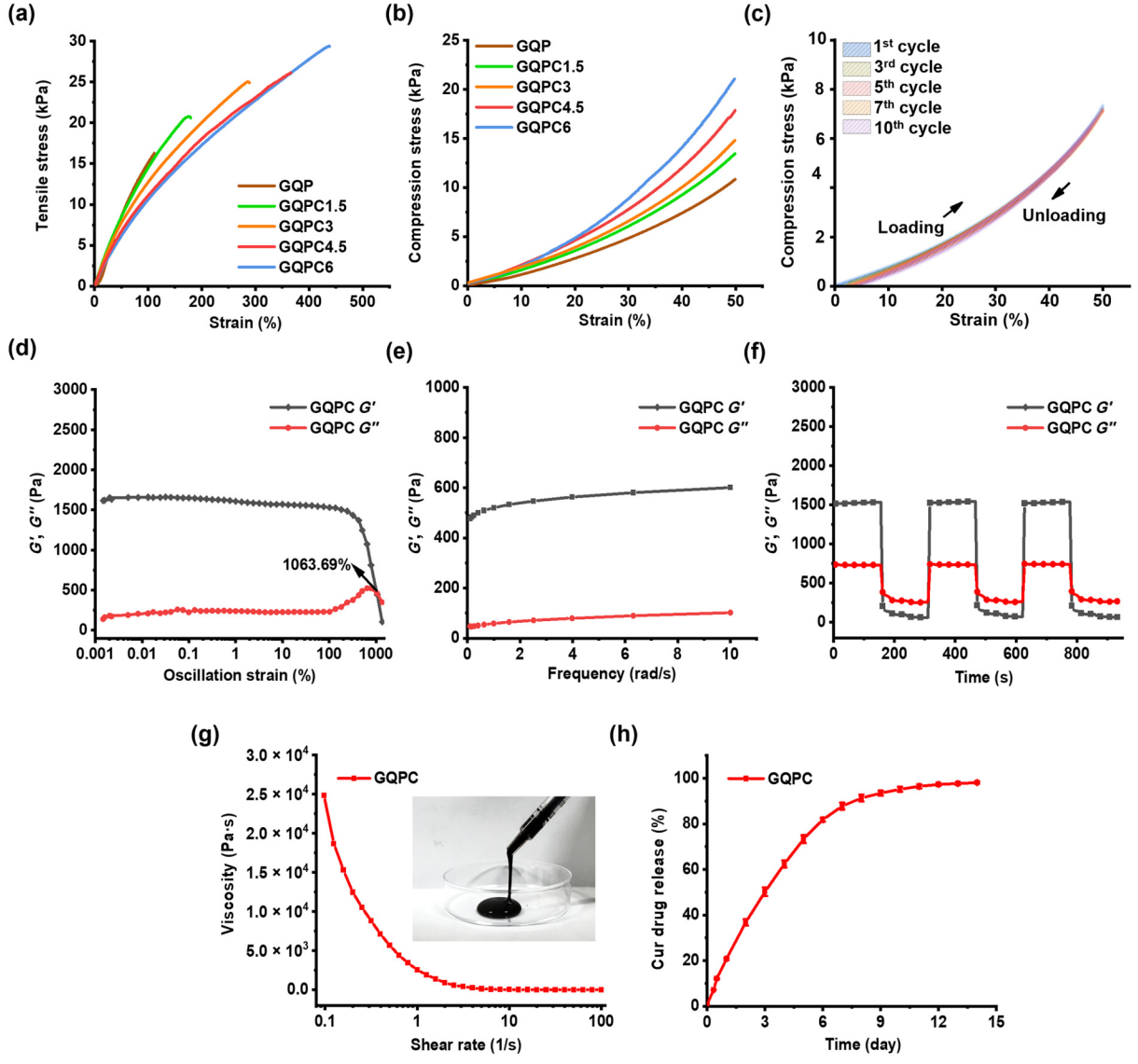


**Figure 3** Mechanical properties and rheological properties of hydrogels, and *in vitro* release of Cur. (a) Tensile stress-strain curves of hydrogels. (b) Compressive stress-strain curves of hydrogels. (c) Loading-unloading cycle curves of GQPC hydrogel under 50% compressive deformation. (d) Strain-dependent oscillatory shear rheological properties of GQPC hydrogel with a fixed frequency of 10 Hz. (e) Dynamic frequency sweep of GQPC hydrogel measured at 0.01% strain. (f) Step-strain measurements of GQPC hydrogel over three cycles at high and low strain, with a frequency of 10 Hz. (g) Shear viscosity of the GQPC hydrogel with a shear rate ranging from 0.1–100 $s^{-1}$ (inset: injectable photo of the GQPC). (h) Release profile of Cur *in vitro*. Data are presented as mean ± SD ($n$ = 3).

39.2% ± 3.5% (Fig. S2 in the ESM). Subsequently, the injured cells were treated with different hydrogel leachates. As shown in Fig. 5(c), the GQPC hydrogel demonstrated significantly greater neuroprotective effects compared to the GQP hydrogel, which could be attributed to the sustained release of Cur from the GQPC hydrogel.

### 3.7 Evaluation of the macrophage polarization effect of hydrogel *in vitro*

It is well known that macrophages play a pivotal role in regulating the repair and regeneration of injured tissues [43]. Macrophages are generally classified into two phenotypes, M1 and M2, which together shape the immune microenvironment of injured tissues. M1-type macrophages secrete large amounts of pro-inflammatory cytokines, such as IL-1$\beta$ and TNF-$\alpha$, which recruit peripheral immune cells and exacerbate secondary injury. In contrast, M2-type macrophages release anti-inflammatory cytokines, such as IL-10, which promotes tissue repair and regeneration after injury [44]. To investigate the modulatory effects of our hydrogels on macrophage polarization, we performed immunofluorescence staining for CD86 and CD206 to mark M1 and M2 phenotypes, respectively, and evaluated IL-1$\beta$, TNF-$\alpha$, and IL-10 levels in RAW264.7 cells using an ELISA kit after LPS and IFN-$\gamma$ treatment.

The RAW264.7 (M0) cells were first polarized to M1 by treating with LPS and IFN-$\gamma$. Following treatment with both GQP and GQPC hydrogel leachates, CD86 expression on RAW264.7 cells was down-regulated compared with the untreated group, indicating that the GQPC hydrogel could inhibit macrophage polarization to M1 (Figs. 6(a) and 6(b)). After RAW264.7 cells were polarized to M1, they were treated with IL-4, GQP, and GQPC hydrogel leachates, respectively. We found that CD206 expression was up-regulated in all groups (Figs. 6(c) and 6(d)), indicating that the

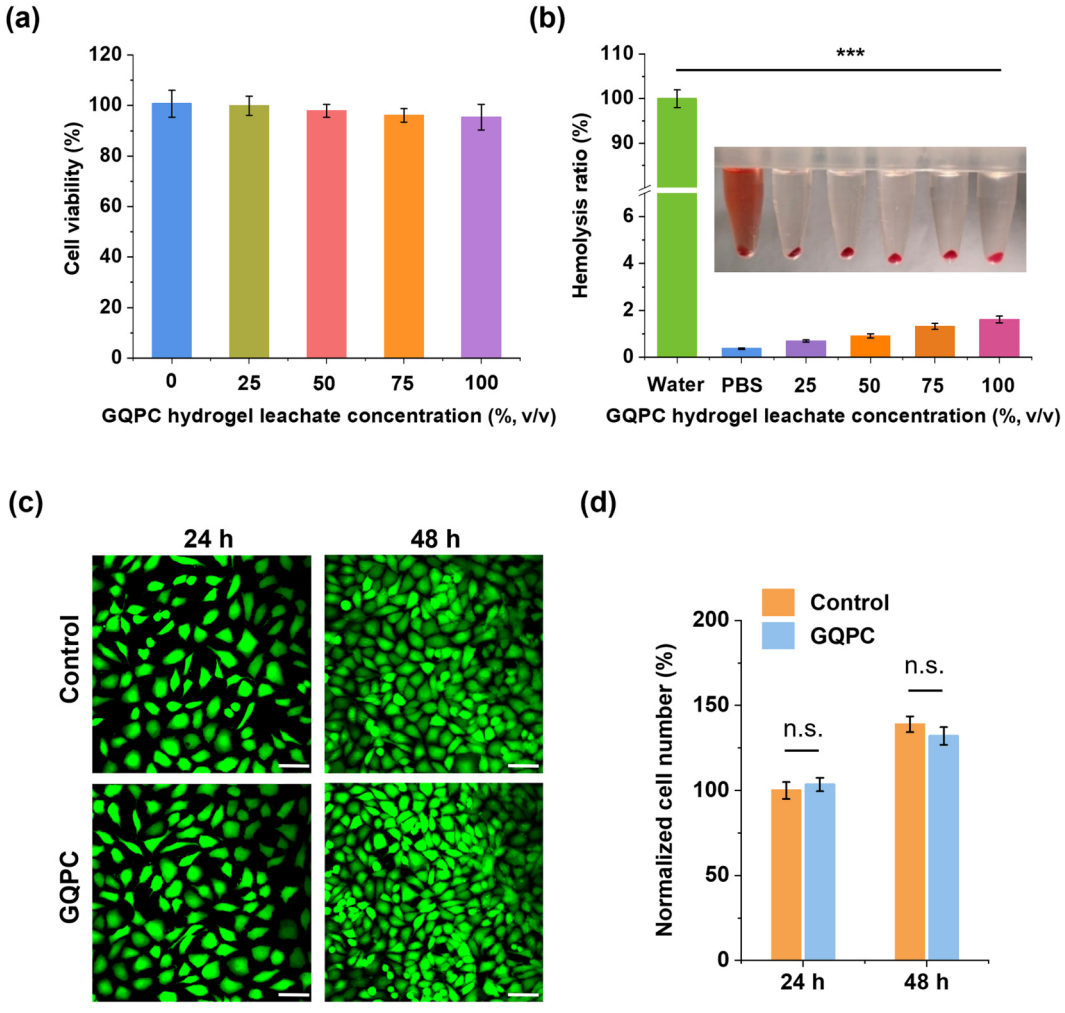


**Figure 4** Evaluation of *in vitro* biocompatibility of GQPC hydrogel. (a) Cytotoxicity of different concentrations of GQPC hydrogel leachate to PC12 cells. Data are presented as mean ± SD ($n$ = 6). (b) Hemolytic activity of different concentrations of GQPC hydrogel leachate to mouse erythrocytes (inset: photos of hemolysis by different concentrations of GQPC hydrogel leachate). (c) Images of live-dead staining of PC12 cells by GQPC hydrogel leachate at different time points and (d) quantification. Scale bars: 50 μm. Data are presented as mean ± SD ($n$ = 3) in panels (b) and (d). ***$P$ < 0.001; n.s.: not significant.

GQP and GQPC hydrogels could promote polarization of RAW264.7 cells from M1 to M2, and the GQPC hydrogel was more effective than the GQP hydrogel. In addition, both hydrogels significantly downregulated pro-inflammatory IL-1$\beta$ and TNF-$\alpha$ levels (Figs. 6(e) and 6(f)).

The IL-1$\beta$ and TNF-$\alpha$ levels in the GQPC hydrogel group were higher than those of the GQP hydrogel and were closer to those in the control group, indicating that the GQPC hydrogel has stronger activity to inhibit inflammation. While the anti-inflammatory IL-10 level was up-regulated (Fig. 6(g)), suggesting that the phenotype of RAW264.7 cells shifted from pro-inflammatory to anti-inflammatory type. Collectively, these findings demonstrated that GQPC hydrogel can effectively promote M1-to-M2 macrophage polarization *in vitro*. Therefore, it might be feasible to achieve the goal of creating a favorable immune microenvironment for spinal cord repair by reducing the inflammatory response following SCI.

### 3.8 Therapeutic effect of hydrogel on SCI rats

Given the superior *in vitro* antioxidant and anti-inflammatory effects of GQPC hydrogel, we explored its use to repair SCI. We first established a rat model of SCI using the weight-drop method and conducted *in vivo* experiments of SCI repair following the schematic outline in Fig. 7(a). All rats exhibited complete hindlimb paralysis immediately after surgery (BBB score = 0, Fig. 7(b)). For the saline-treated group, the rats displayed limited motor recovery at the fourth week with BBB scores below 4, indicating minimal intrinsic neural repair. In contrast, the rats treated with GQP and GQPC hydrogels showed accelerated motor function recovery, and the GQPC group achieved the most significant restoration of motor abilities and the highest BBB scores. Consistent with BBB assessments, photographs of hind limb recovery, gait analysis, and spinal cord tissues of injured segments also revealed notable differences among groups (Fig. 7(c)). The rats in the saline group dragged their hind limbs, resulting in irregular and disorganized footprints. The rats in the GQP group exhibited moderate plantar support but still showed hind limb dragging. The rats treated with GQPC hydrogel displayed clear and well-defined footprints without dragging, which were closer to those of the uninjured control group. The overlap of hindlimb and forelimb footprints during walking suggested improved interlimb coordination in the GQPC group. Additionally, the GQPC group showed significantly reduced SCI at the lesion site and exhibited excellent connectivity and integration between the injury region and surrounding normal tissue. After 28 days of implantation, no hydrogel residue was

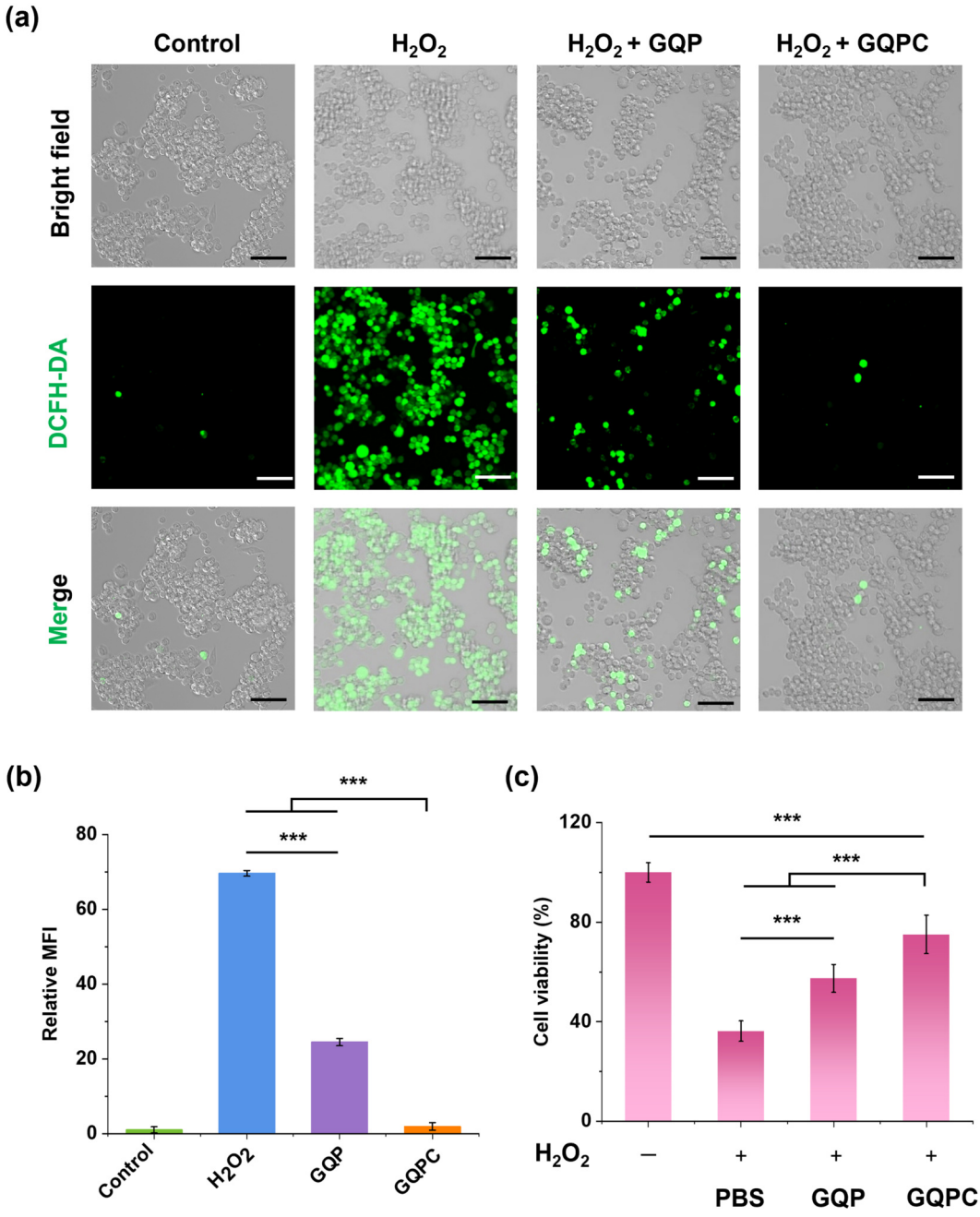


**Figure 5** Evaluation of *in vitro* antioxidant capacity of GQPC hydrogel. (a) Images of intracellular ROS levels in RAW264.7 cells treated by $H_2O_2$ and hydrogel leachates, and (b) quantification. Scale bars: 50 μm. MFI: mean fluorescence intensity. Data are presented as mean ± SD ($n = 3$). ***$P < 0.001$. (c) Evaluation of SH-SY5Y cell survival after intervention with 400 μM $H_2O_2$ and simultaneous incubation with different hydrogel leachates, respectively. Data are presented as mean ± SD ($n = 6$). ***$P < 0.001$.

observed in the extracted spinal cord tissue, and the newborn tissue completely replaced the GQPC hydrogel. Additional functional assessments, including the inclined plane test (Fig. 7(d)) and grid crawl test (Fig. S3 in the ESM), confirmed varying degrees of hindlimb motor recovery 28 days post-treatment, and the GQPC hydrogel group demonstrated the most substantial improvement. These results indicated that the GQPC hydrogel could promote SCI repair and exhibit promising potential for clinical therapy of SCI.

Evidence shows that cystic cavities and neural demyelination often occur at the injury site during the SCI regeneration and repair process [45], thereby affecting neurological function recovery after SCI. We performed H&E staining to evaluate the cystic cavity of therapeutic SCI. As shown in Fig. 7(e), a prominent cavity was observed in the saline-treated group on the 28th day post-injury, indicating the limited self-repair capacity of the spinal cord in these rats. In contrast, the cavity area was significantly reduced in both the GQP and GQPC groups, with the GQPC group exhibiting almost complete absence of cavity formation. Given that the integrity of the myelin sheath is a critical factor for effective axonal conduction, we performed LFB staining to evaluate neural demyelination. Figure 7(f) revealed a significant decrease in cavity area and an obvious increase in bright blue myelin tissue in both GQP and GQPC-treated groups compared to the saline-treated group. The GQPC group showed a more pronounced increase in

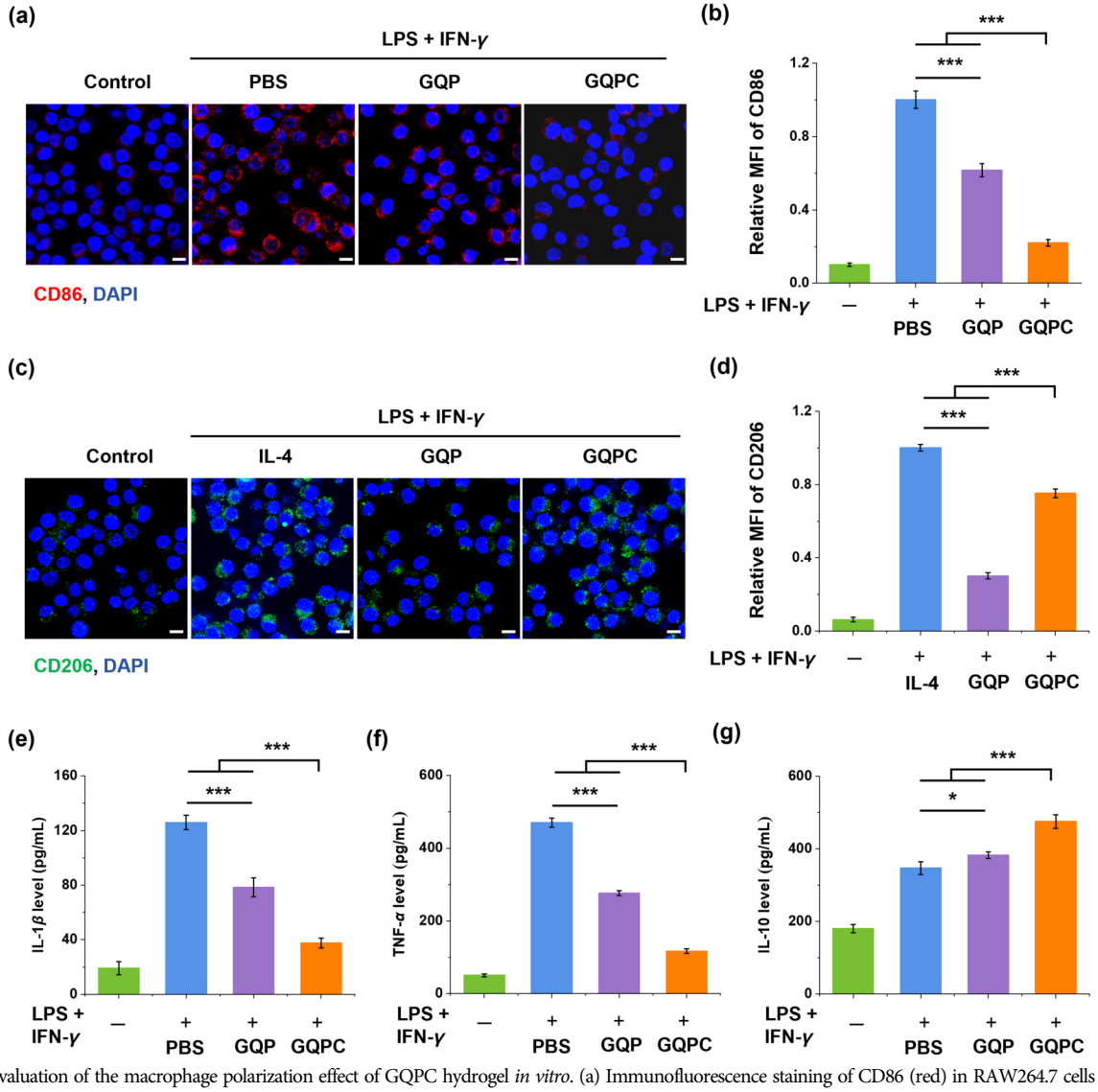


**Figure 6** Evaluation of the macrophage polarization effect of GQPC hydrogel *in vitro*. (a) Immunofluorescence staining of CD86 (red) in RAW264.7 cells treated with different materials and (b) quantification. Scale bars: 10 μm. (c) Immunofluorescence staining of CD206 (green) in RAW264.7 cells treated with different materials and (d) quantification. Scale bars: 10 μm. (e) IL-1$\beta$ levels, (f) TNF-$\alpha$ levels, and (g) IL-10 levels in RAW264.7 cells. Data are presented as mean ± standard deviation ($n$ = 3) in panels (b), (d), and (e)–(g). *$P$ < 0.05 and ***$P$ < 0.001.

myelin content, demonstrating that this hydrogel could effectively promote myelin sheath repair of SCI. In conclusion, the above results confirmed that the GQPC hydrogel could be used to repair SCI tissue and thereby enhance motor function recovery of SCI rats.

### 3.9 Evaluation of macrophage modulation and anti-oxidative stress effect *in vivo*

The local immune microenvironment of SCI plays a vital role in neural regeneration. Thus, early suppression of inflammation is crucial to create a favorable immune microenvironment for SCI repair. To assess the modulatory effects of the hydrogels on macrophage polarization *in vivo*, we performed immunofluorescence staining and measured inflammatory cytokine levels of spinal cord tissues on the 7$^{th}$ day post-surgery. As shown in Figs. 8(a)–8(d), expression of the M2 macrophage marker CD206 in the GQPC-treated group was significantly higher than in the GQP and saline control groups. In contrast, the expression of the M1 macrophage marker CD86 was markedly lower. These results indicated that the GQPC hydrogel *in vivo* more effectively promoted macrophage polarization from the pro-inflammatory M1 to the anti-inflammatory M2 type than the GQP hydrogel. Consistent with these findings, pro-inflammatory cytokines IL-1$\beta$ and TNF-$\alpha$ were significantly down-regulated (Figs. 8(e) and 8(f)), whereas the anti-inflammatory cytokine IL-10 was elevated (Fig. 8(g)) after GQPC treatment. Overall, these results demonstrated that the GQPC hydrogel effectively suppressed early inflammation and remodeled the inflammatory microenvironment after SCI.

Oxidative damage caused by a highly oxidative stress microenvironment is a key factor contributing to neural tissue injury and impeding spinal cord regeneration [46]. To evaluate the antioxidant capacity of the hydrogels, we measured levels of oxidative stress markers, including SOD, GSH-Px, and MDA. As shown in Figs. S4(a)–S4(c) in the ESM, SOD and GSH-Px levels increased after treatment with both GQP and GQPC hydrogels,

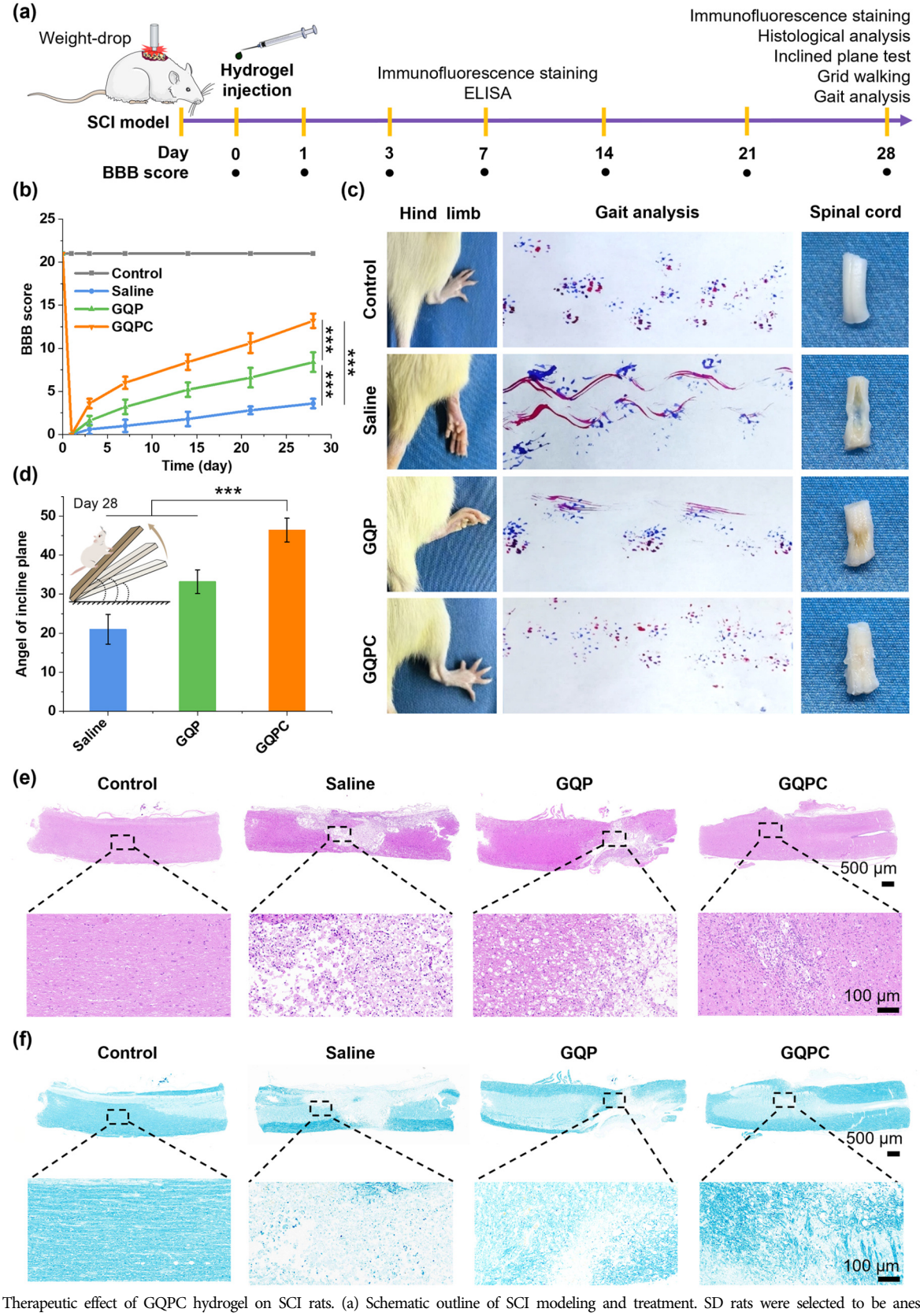


**Figure 7** Therapeutic effect of GQPC hydrogel on SCI rats. (a) Schematic outline of SCI modeling and treatment. SD rats were selected to be anesthetized by intraperitoneal injection of pentobarbital sodium, and the spinal cord of the T9 segment of rats was injured by the weight-drop method. (b) BBB scores of rats of various groups after SCI modeling and treatment. (c) Photographs of the recovery of hind limbs, gait analysis, and spinal cord tissues of injured segments, which were removed from rats of different groups on the 28th day. (d) The maximum angle value of the inclined plane is obtained when sliding out of the inclined plane on the 28th day after SCI modeling. (e) Images of H&E-staining and (f) LFB-staining of spinal cord tissues on the 28th day. Data are presented as mean ± SD ($n$ = 5) in panels (b) and (d). ***$P$ < 0.001.

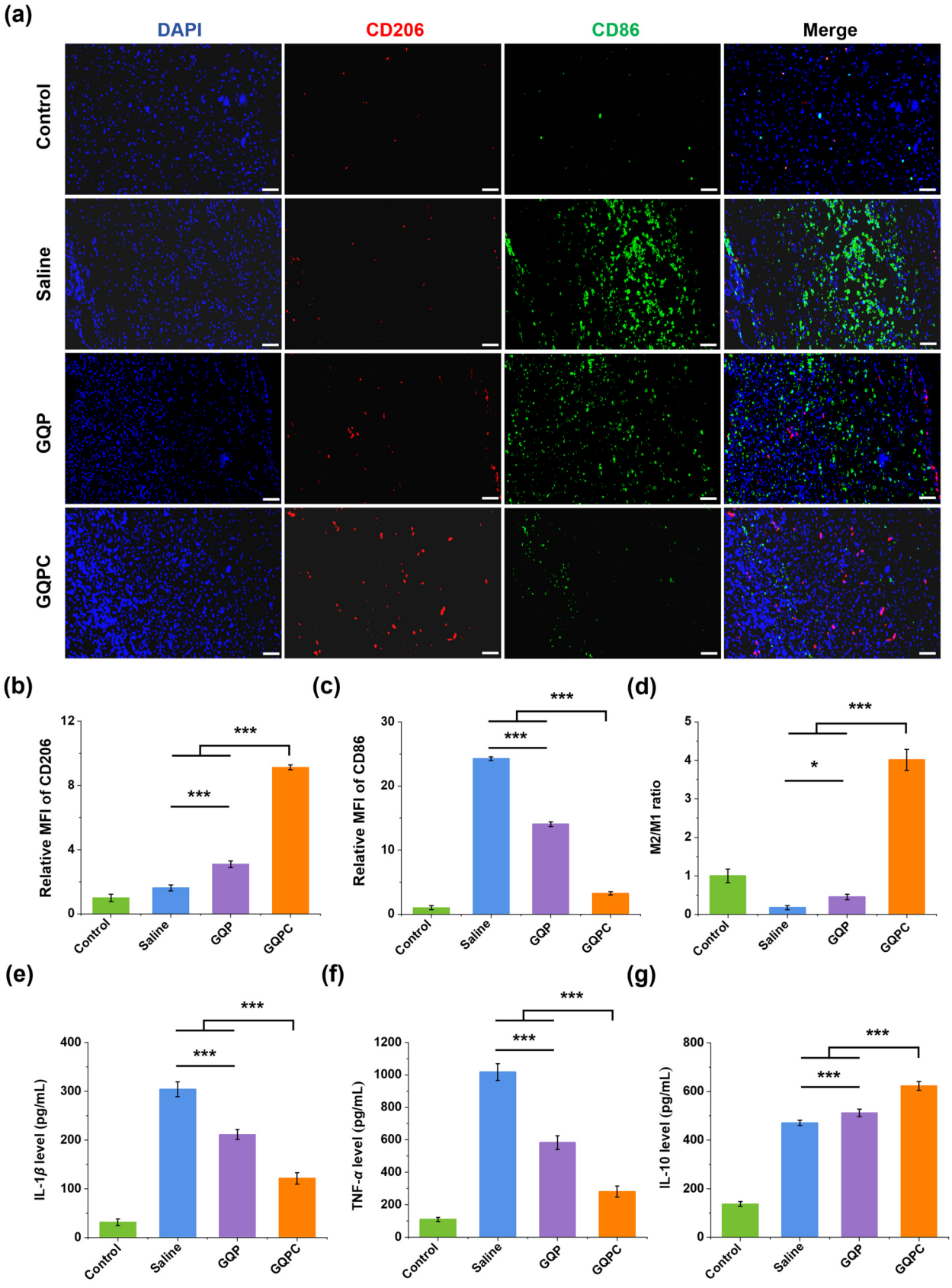


**Figure 8** Evaluation of the macrophage polarization effect of GQPC hydrogel *in vivo*. (a)–(d) Evaluation of macrophage polarization by immunofluorescence staining of CD86 (M1-type macrophage marker) and CD206 (M2-type macrophage marker) staining after 7 days of treatment in different groups and quantitative analysis. Scale bars: 100 μm. (e) Evaluation of IL-1$\beta$ level, (f) TNF-$\alpha$ level, and (g) IL-10 level in spinal cord tissues after 7 days of treatment in different groups by ELISA kit. Data are presented as mean ± SD ($n = 5$) in panels (b)–(g). $^{*}P < 0.05$ and $^{***}P < 0.001$.

while MDA levels decreased. Importantly, the levels of these markers in the GQPC group were closest to those observed in the uninjured control group, indicating that GQPC hydrogel significantly alleviated oxidative stress at the site of the SCI. This antioxidant effect should be primarily attributed to the presence of Cur. Together with the results of macrophage modulation, GQPC hydrogel not only remodeled the inflammatory microenvironment but also effectively attenuated early oxidative stress *in vivo* to create a favorable microenvironment for spinal cord repair and neural regeneration.

### 3.10 Inhibition of glial scar formation and promotion of axonal and neural regeneration

SCI induces astrocyte proliferation, leading to the formation of neuroglial scars that act as physical barriers to prevent axonal reconnection [47]. Therefore, we evaluated glial scar formation at the injury site in spinal cord tissue by immunofluorescence staining for GFAP, a well-established marker of astrocytes. As shown in Figs. 9(a) and 9(b), astrocytes were significantly suppressed after treatment with both GQP and GQPC compared with the saline-treated group, and the GQPC hydrogel more effectively minimized astrocyte proliferation, indicating that the GQPC hydrogel is more effective in reducing glial scar formation. Furthermore, immunostaining for NeuN (red), which is a marker of mature neurons, revealed that the proportion of NeuN-positive cells in the injured area of SCI treated with the GQPC group was higher compared with the saline group and the GQP group (Figs. 9(a) and 9(c)). These results demonstrated that the GQPC hydrogel had a stronger function to enhance neuron regeneration at the injury site.

To further assess the ability of the hydrogel to promote neural regeneration, we performed immunofluorescence staining of

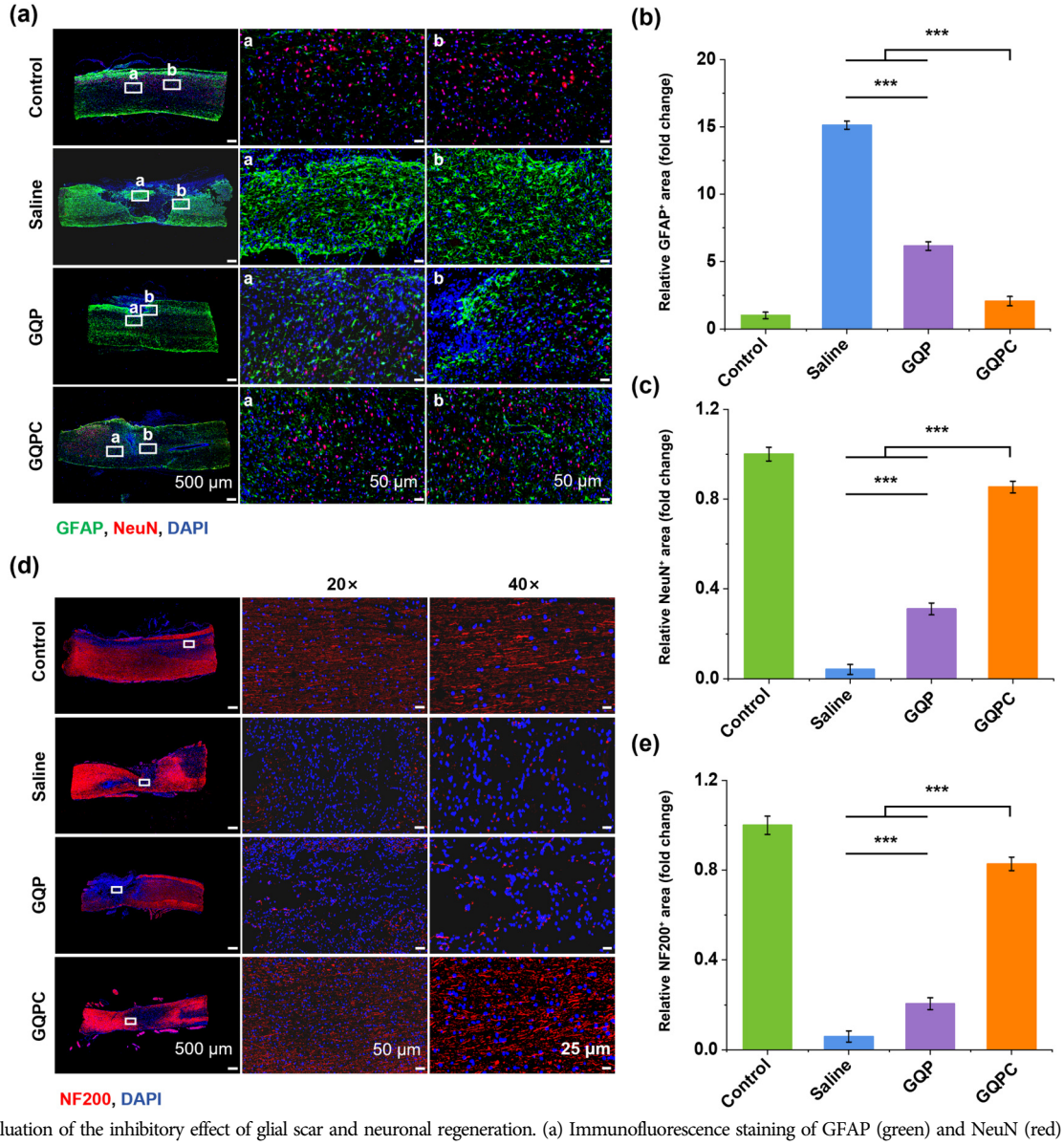


**Figure 9** Evaluation of the inhibitory effect of glial scar and neuronal regeneration. (a) Immunofluorescence staining of GFAP (green) and NeuN (red) in the injured spinal cord of different treatment groups on the 28th day postoperatively. (b) Quantification of the percentage of GFAP-positive area in the injured spinal cord. (c) Quantification of the percentage of NeuN-positive area in injured spinal cord tissues. (d) Immunofluorescence staining of NF-200 (red) in the injured spinal cord of different treatment groups on the 28th day postoperatively. (e) Quantification of the percentage of NF-200-positive area in the injured spinal cord. Data are presented as mean ± standard deviation ($n = 5$) in panels (b), (c), and (e). $^{*}P < 0.05$ and $^{***}P < 0.001$.

NF200, which is predominantly expressed in central nervous system axons, to evaluate the axonal regeneration. As shown in Figs. 9(d) and 9(e), NF200 fluorescence intensity markedly increased in both the GQP and GQPC groups compared to the saline-treated group, with the GQPC group exhibiting the highest intensity of neural fibers. These results indicated that the GQPC hydrogel effectively enhanced axonal regeneration, thereby accelerating spinal cord repair.

### 3.11 Mechanism of GQPC hydrogel in neural regeneration and microenvironment targeting

Our results demonstrate that the GQPC hydrogel promotes neural regeneration after SCI through synergistic actions of its components, particularly Cur and PDA, spanning microenvironment modulation, neuroprotection, and structural repair. Consistent with multimodal repair cascades reported previously [48], PDA provides an early antioxidant barrier that, together with sustained Cur release, scavenges excessive ROS and alleviates oxidative damage. Cur further exerts immunomodulatory effects by promoting macrophage polarization toward the M2 phenotype and suppressing glial scar formation. In agreement with Zhu et al. [49], these effects likely involve regulation of inflammatory signaling pathways, including inhibition of nuclear factor-$\kappa$B (NF-$\kappa$B)-mediated transcription of pro-inflammatory mediators (e.g., TNF-$\alpha$, IL-1$\beta$) and activation of PPAR-$\gamma$/STAT6 pathways that favor anti-inflammatory polarization and restrain astrocyte activation. Cur has also been reported to activate the Nrf2/HO-1 antioxidant pathway, enhancing endogenous cellular protection [50]. Collectively, these molecular and cellular effects translate into reduced neuronal apoptosis, improved axonal regeneration and remyelination, and partial recovery of neural circuitry and motor function.

From a materials design perspective, this mechanism aligns with the emerging paradigm of hydrogels targeting pathological microenvironments. Pathology-responsive systems exploit local signals such as oxidative stress or inflammation to improve therapeutic precision and minimize off-target effects. For instance, studies have demonstrated on-demand release of anti-inflammatory drugs through pathological microenvironment response [51], or targeted immune reprogramming in oxidative microenvironments to promote tissue repair [52]. Examples of pathological response hydrogels utilizing pathological signals like hydrogen peroxide as triggers have also been reported [53]. Although the GQPC hydrogel is not a switch-responsive system, its design logic is analogous: SCI lesions feature elevated ROS and inflammation, where sustained Cur release combined with PDA antioxidant activity remodels the local inflammatory profile, promotes M2 polarization, suppresses scarring, and facilitates regeneration. Thus, this work represents a functionally synergistic hydrogel strategy that targets key pathological events, oxidative stress, and immune imbalance as central intervention points.

## 4 Conclusions

In this study, we developed a Gel/QCS/PDA multifunctional hydrogel loaded with Cur for the treatment of SCI. The hydrogel exhibited suitable mechanical properties matching those of spinal cord tissue, self-healing properties, and injectability with Cur released continuously over 14 days. *In vitro* experiments demonstrated that the hydrogel had outstanding biocompatibility, significantly alleviating oxidative stress and promoting the polarization of pro-inflammatory M1 macrophages to the anti-inflammatory M2 phenotype. Upon injection into the lesion of SCI, the hydrogel could alleviate early oxidative stress and facilitate macrophage phenotype switching, remodeling the immune microenvironment to effectively inhibit glial scar formation, and accelerate axonal and neural regeneration. The GQPC hydrogel showed promising potential for the clinical treatment of SCI. In conclusion, this study presented an effective therapeutic platform for SCI and other central nervous system disorders.

**Electronic Supplementary Material**: Supplementary material (self-healing properties of the hydrogel, cytotoxicity of SH-SY5Y cells after $H_2O_2$ stimulation, expression of antioxidant enzymes, and grid-walking test) is available in the online version of this article at https://doi.org/10.26599/NR.2026.94908574.

## Data availability

All data needed to support the conclusions in the paper are presented in the manuscript and the Electronic Supplementary Material. Additional data related to this paper may be requested from the corresponding author upon request.

## Acknowledgements

This work was financially supported by the National Key Research and Development Program of China (No. 2020YFA0710801), Tianjin Science and Technology Program Project (No. 24JCYBJC01940), and the Directional Institutionalized Scientific Research Platform relies on the Beijing Synchrotron Radiation Facility of the Chinese Academy of Sciences (No. JZHKYPT-2021-02). Additionally, the authors express their gratitude to the participants for their contributions.

## Declaration of competing interest

All the contributing authors report no conflict of interests in this work.

## Author contribution statement

Y. Y. H.: Methodology, formal analysis, investigation, validation, data curation, writing – original draft. Y. X. J.: Investigation, formal analysis, data curation, writing – original draft. X. Y. N.: Formal analysis, data curation. Y. H. L.: Data curation, investigation. T. Z.: Supervision, conceptualization. H. T. R., Y. Y., L. Y. W.: Conceptualization, supervision, writing – original draft, writing – review & editing.

## Informed consent

Not applicable.

## Ethics statement

The animal experiments were carried out following the guidelines of the Nankai University Institutional Committee for the Care and Use of Laboratory Animals and were approved by the Committee on Ethical Use of Animals of Nankai University (Approval No. 2024-SYDWLL-000642).

## Use of AI statement

The authors used DeepSeek exclusively for language editing to improve clarity and grammar. The scientific content, interpretation, and conclusions were developed entirely by the authors. After using this tool/service, the authors reviewed and edited the content as needed and take full responsibility for the content of the publication.

## References


[1] Hilton, B. J.; Griffin, J. M.; Fawcett, J. W.; Bradke, F. Neuronal maturation and axon regeneration: Unfixing circuitry to enable repair. *Nat. Rev. Neurosci.* **2024**, *25*, 649–667.

[2] Ai, Y. X.; Hu, C. P.; Wang, Y. F.; Liu, Y.J.; Liu, R. F.; Xu, H. L.; Li, H.; Zhao, Y. Q.; Wang, Y. H.; Ning, R. J. et al. Core-shell hydrogel microspheres with sequential delivery of cerium oxide nanoparticles and spinal white matter extracellular matrix for improved functional recovery in spinal cord injury. *Chem. Eng. J.* **2025**, *508*, 160861.

[3] Sofroniew, M. V. Dissecting spinal cord regeneration. *Nature* **2018**, *557*, 343–350.

[4] Badhiwala, J. H.; Wilson, J. R.; Witiw, C. D.; Harrop, J. S.; Vaccaro, A. R.; Aarabi, B.; Grossman, R. G.; Geisler, F. H.; Fehlings, M. G. The influence of timing of surgical decompression for acute spinal cord injury: A pooled analysis of individual patient data. *Lancet Neurol.* **2021**, *20*, 117–126.

[5] Lindsay, S. L.; McCannney, G. A.; Willison, A. G.; Barnett, S. C. Multi-target approaches to CNS repair: Olfactory mucosa-derived cells and heparan sulfates. *Nat. Rev. Neurol.* **2020**, *16*, 229–240.

[6] James, N. D.; McMahon, S. B.; Field-Fote, E. C.; Bradbury, E. J. Neuromodulation in the restoration of function after spinal cord injury. *Lancet Neurol.* **2018**, *17*, 905–917.

[7] Zhang, S. L.; Ran, Y. Y.; Tuolhen, Y.; Wang, Y. F.; Tian, G.Q.; Xi, J. N.; Feng, Z. G.; Su, W.; Ye, L.; Liu, Z. J. Curcumin loaded hydrogel with double ROS-scavenging effect regulates microglia polarization to promote poststroke rehabilitation. *Mater. Today Bio* **2024**, *28*, 101177.

[8] David, G.; Mohammadi, S.; Martin, A. R.; Cohen-Adad, J.; Weiskopf, N.; Thompson, A.; Freund, P. Traumatic and nontraumatic spinal cord injury: Pathological insights from neuroimaging. *Nat. Rev. Neurol.* **2019**, *15*, 718–731.

[9] Flack, J. A.; Sharma, K. D.; Xie, J. Y. Delving into the recent advancements of spinal cord injury treatment: A review of recent progress. *Neural Regen. Res.* **2022**, *17*, 283–291.

[10] Ko, W. K.; Kim, S. J.; Jo, M. J.; Choi, H.; Lee, D.; Kwon, I. K.; Lee, S. H.; Han, I. B.; Sohn, S. Ursodeoxycholic acid inhibits inflammatory responses and promotes functional recovery after spinal cord injury in rats. *Mol. Neurobiol.* **2019**, *56*, 267–277.

[11] Feng, F.; Song, X. Y.; Tan, Z.; Tu, Y. J.; Xiao, L. Y.; Xie, P. F.; Ma, Y. H.; Sun, X. M.; Ma, J. W.; Rong, L. M. et al. Cooperative assembly of a designer peptide and silk fibroin into hybrid nanofiber gels for neural regeneration after spinal cord injury. *Sci. Adv.* **2023**, *9*, eadg0234.

[12] Liu, J. L.; Yao, Z. H.; Hu, Z. J.; Zhang, X. D.; Gong, B. W.; Dai, Y.; Weng, H. Y.; Xiao, L. Y.; Zhang, B. B.; Li, T. et al. Spatiotemporal delivery of required facilitators for microenvironment remodeling propels neural regeneration after spinal cord injury. *Adv. Mater.* **2025**, *28*, e03479.

[13] Xiao, L. Y.; Shi, K. X.; Li, W.; Liu, J. L.; Xie, P. F.; Hu, Z. J.; Dai, Y.; Weng, H. Y.; Yuan, Q. J.; Wu, W. T. et al. Targeting fibrotic scarring by mechanoregulation of Il11ra1$^{+}$/Itga11$^{+}$ fibroblast patterning promotes axon growth after spinal cord injury. *Adv Sci.* **2025**, *12*, e13476.

[14] Zheng, B. W.; Ge, M. P.; Zhang, J.; Zhu, T.; Yi, Y.; Rong, H. T. Biomembrane delivers neurotrophic factor for spinal cord injury recovery through microneedle patch. *Chem. Eng. J.* **2025**, *520*, 166198.

[15] Lin, X. Y.; Lai, B. Q.; Zeng, X.; Che, M. T.; Ling, E. A.; Wu, W. T.; Zeng, Y. S. Cell transplantation and neuroengineering approach for spinal cord injury treatment: A summary of current laboratory findings and review of literature. *Cell Transplant.* **2016**, *25*, 1425–1438.

[16] Han, Y.; Yang, J. L.; Zhao, W. W.; Wang, H. M.; Sun, Y. L.; Chen, Y. J.; Luo, J.; Deng, L. F.; Xu, X. Y.; Cui, W. G. et al. Biomimetic injectable hydrogel microspheres with enhanced lubrication and controllable drug release for the treatment of osteoarthritis. *Bioact. Mater* **2021**, *6*, 3596–3607.

[17] Nazemi, Z.; Nourbakhsh, M. S.; Kiani, S.; Heydari, Y.; Ashtiani, M. K.; Daemi, H.; Baharvand, H. Co-delivery of minocycline and paclitaxel from injectable hydrogel for treatment of spinal cord injury. *J. Controlled Release* **2020**, *321*, 145–158.

[18] Yang, Y. M.; Fan, Y. H.; Zhang, H. P.; Zhang, Q.; Zhao, Y. N.; Xiao, Z.F.; Liu, W. B.; Chen, B.; Gao, L.; Sun, Z. et al. Small molecules combined with collagen hydrogel direct neurogenesis and migration of neural stem cells after spinal cord injury. *Biomaterials* **2021**, *269*, 120479.

[19] Luo, J. H.; Shi, X. S.; Li, L. M.; Tan, Z.; Feng, F.; Li, J.; Pang, M.; Wang, X. Y.; He, L. M. An injectable and self-healing hydrogel with controlled release of curcumin to repair spinal cord injury. *Bioact. Mater.* **2021**, *6*, 4816–4829.

[20] Liu, Y.; Hsu, Y. H.; Huang, A. P. H.; Hsu, S. H. Semi-interpenetrating polymer network of hyaluronan and chitosan self-Healing hydrogels for central nervous system repair. *ACS Appl. Mater. Interfaces* **2020**, *12*, 40108–40120.

[21] Fan, C. X.; Yang, W.; Zhang, L. L.; Cai, H.; Zhuang, Y.; Chen, Y. Y.; Zhao, Y. N.; Dai, J. W. Restoration of spinal cord biophysical microenvironment for enhancing tissue repair by injury-responsive smart hydrogel. *Biomaterials* **2022**, *288*, 121689.

[22] Hou, P.; Lei, K.; Zhang, Z. S.; Zhao, P. C.; Li, J. H.; Li, G. D.; Bao, J. F.; Li, X.; Xue, Y.; Quan, C. S. et al. Adhesive transparent antimicrobial quaternized chitosan/oxidized dextran/polydopamine nanoparticle hydrogels for accelerated wound healing. *Biomater. Adv.* **2025**, *169*, 214176.

[23] Shi, T. B.; Chen, Y.; Zhou, L. Q.; Wu, D. W.; Chen, Z.; Wang, Z.Y.; Sun, L.; Lin, J. X.; Liu, W. G. Carboxymethyl cellulose/quaternized chitosan hydrogel loaded with polydopamine nanoparticles promotes spinal cord injury recovery by anti-ferroptosis and M1/M2 polarization modulation. *Int. J. Biol. Macromol.* **2024**, *275*, 133484.

[24] Mao, J. S.; Chen, L. L.; Zhuang, G. Y.; Jin, Z. Q.; Wu, S. K.; Ying, M. S.; Sheng, L. C.; Lv, J. W.; Bi, Q. C.; Ye, J. J. Curcumin-loaded polydopamine nanoparticles-based antioxidant scaffold promote spinal cord repair though dural-regulation of macrophage polarization. *Mater. Today Bio* **2025**, *32*, 101895.

[25] Li, W. C.; Yao, S. P.; Li, H. R.; Meng, Z. D.; Sun, X. R. Curcumin promotes functional recovery and inhibits neuronal apoptosis after spinal cord injury through the modulation of autophagy. *J. Spinal Cord Med.* **2021**, *44*, 37–45.

[26] Lee, S.; Cho, D. C.; Han, I.; Kim, K. T. Curcumin as a promising neuroprotective agent for the treatment of spinal cord injury: A review of the literature. *Neurospine* **2022**, *19*, 249–261.

[27] Su, H. W.; Ma, Y. Y.; Li, W. H.; Ren, H. Y.; Maimaitikelimu, X.; Lin, F. S. Y.; Zhang, H. B.; Liu, S.; Chen, Q. C.; Wang, H. Hierarchical gelatin-derived hydrogel film with reactive oxygen species scavenging properties for spinal cord injury repair. *Chem. Eng. J.* **2025**, *503*, 158134.

[28] Farzan, M.; Soleimannejad, M.; Shariat, S.; Heidari Sureshjani, M.; Gholipour, A.; Ashrafi Dehkordi, K.; Alerasoul Dehkordi, S. M. R.; Farzan, M. A biomimetic injectable chitosan/alginate hydrogel biocopmosites encapsulating selenium-folic acid nanoparticles for regeneration of spinal cord injury: An *in vitro* study. *Int. J. Biol. Macromol.* **2025**, *288*, 138682.

[29] Zhu, Y. J.; Xiu, Z. L.; Jiang, X. X.; Zhang, H. F.; Li, X. F.; Feng, Y. R.; Li, B. J.; Cai, R.; Li, C. H.; Tao, G. Injectable hydrogels with ROS-triggered drug release enable the co-delivery of antibacterial agent and anti-inflammatory nanoparticle for periodontitis treatment. *J. Nanobiotechnol.* **2025**, *23*, 205.

[30] Wan, Y. J.; Lin, Y.; Tan, X.; Gong, L. Y.; Lei, F.; Wang, C. G.; Sun, X. D.; Du, X. J.; Zhang, Z. R.; Jiang, J. et al. Injectable hydrogel to deliver bone mesenchymal stem cells preloaded with azithromycin to promote spinal cord repair. *ACS Nano* **2024**, *18*, 8934–8951.

[31] Li, R. X.; Hu, Y. Q.; Hou, Y. Y.; Li, J. G.; Niu, X. Y.; Wang, M. D.; Wang, L. Y. Receptor-mediated membrane fusion drug delivery system based on chitosan derivatives to enhance tumor chemotherapy. *Int. J. Biol. Macromol.* **2025**, *311*, 143869.

[32] Du, X. C.; Zhao, X. L.; Liu, Y. D.; Chen, Y. F.; Li, R. X.; Zhang, T. X.; Wang, L. Y. A self-elastic chitosan sponge reinforced with lauric acid-modified quaternized chitosan and attapulgite to treat noncompressible hemorrhage and facilitate wound healing. *Carbohydr. Polym.* **2025**, *351*, 123121.

[33] Mohseni, M.; Shokrollahi, P.; Barzin, J. Impact of supramolecular interactions on delivery of dexamethasone from a physical network of gelatin/ZnHAp composite scaffold. *Int. J. Pharm.* **2022**, *615*, 121520.

[34] Ren, Y. Z.; Zhao, X.; Liang, X. F.; Ma, P. X.; Guo, B. L. Injectable hydrogel based on quaternized chitosan, gelatin and dopamine as localized drug delivery system to treat Parkinson's disease. *Int. J. Biol. Macromol.* **2017**, *105*, 1079–1087.

[35] Iftime, M. M.; Morariu, S.; Marin, L. Salicyl-imine-chitosan hydrogels: Supramolecular architecturing as a crosslinking method toward multifunctional hydrogels. *Carbohydr. Polym.* **2017**, *165*, 39–50.

[36] Wang, Q.; Yan, S. Z.; Ning, Y. J.; Zhu, Y.; Sergeeva, I.; Li, Y.; Qi, B. K. Effect of sodium alginate block type on the physicochemical properties and curcumin release behavior of quaternized chitosan-oxidized sodium alginate Schiff base hydrogels. *Food Chem.* **2024**, *444*, 138688.

[37] Yu, R.; Li, M.; Li, Z. L.; Pan, G. Y.; Liang, Y. Q.; Guo, B. L. Supramolecular thermo-contracting adhesive hydrogel with self-Removability simultaneously enhancing noninvasive wound closure and MRSA-infected wound healing. *Adv. Healthc. Mater.* **2022**, *11*, 2102749.

[38] Hou, Y. Y.; Huang, H. B.; Gong, W.; Wang, R.; He, W. Y.; Wang, X. C.; Hu, J. N. Co-assembling of natural drug-food homologous molecule into composite hydrogel for accelerating diabetic wound healing. *Biomater. Adv.* **2022**, *140*, 213034.

[39] Geng, H. M.; Li, Z. W.; Li, Z.; Zhang, Y. Q.; Gao, Z. L.; Sun, L.; Li, X. G.; Cui, J. W.; Ni, S. L.; Hao, J. C. Restoring neuronal iron homeostasis revitalizes neurogenesis after spinal cord injury. *Proc. Natl. Acad. Sci. USA* **2023**, *120*, e2220300120.

[40] Chen, Z. N.; Zhang, H. M.; Fan, C. X.; Zhuang, Y.; Yang, W.; Chen, Y. Y.; Shen, H.; Xiao, Z. F.; Zhao, Y. N.; Li, X. R. et al. Adhesive, stretchable, and spatiotemporal delivery fibrous hydrogels harness endogenous neural stem/progenitor cells for spinal cord injury repair. *ACS Nano* **2022**, *16*, 1986–1998.

[41] Liu, Q.; Wang, W. S.; Yang, H. M.; Wang, Y. J.; Shi, Y. D.; Chen, Y. L.; Luo, D.; Guo, D.; Lin, D. K.; Yue, K. et al. Microenvironment-responsive injectable conductive hydrogel for spinal cord injury repair. *Adv. Funct. Mater.* **2024**, *34*, 2406376.

[42] Meng, J.; Sun, J. J.; Kang, J. L.; Ren, S. L.; Xu, M. M.; Li, R. Z.; Zhao, X. H.; Yuan, Y. T.; Xin, L.; Zhang, R. P. Multifunctional hydrogels loaded with tellurium nanozyme for spinal cord injury repair. *Mater. Today Bio* **2024**, *29*, 101339.

[43] Zhao, C. L.; Yang, Z. Y.; Li, Y. B.; Wen, Z. L. Macrophages in tissue repair and regeneration: Insights from zebrafish. *Cell Regen.* **2024**, *13*, 12.

[44] Jiang, Y. X.; Rong, H. T.; Wang, Y. F.; Liu, S. G.; Xu, P.; Luo, Z.; Guo, L. M.; Zhu, T.; Rong, H. P.; Wang, D. S. et al. Single-atom cobalt nanozymes promote spinal cord injury recovery by anti-oxidation and neuroprotection. *Nano Res.* **2023**, *16*, 9752–9759.

[45] Qi, Z. P.; Pan, S.; Yang, X. Y.; Zhang, R. F.; Qin, C.; Yan, H. Y.; Zhu, L. C.; Kong, W. J. Injectable hydrogel loaded with CDs and FTY720 combined with neural stem cells for the treatment of spinal cord injury. *Int. J. Nanomedicine* **2024**, *19*, 4081–4101.

[46] Zhao, W. Y.; Gasterich, N.; Clarner, T.; Voelz, C.; Behrens, V.; Beyer, C.; Fragoulis, A.; Zendedel, A. Astrocytic Nrf2 expression protects spinal cord from oxidative stress following spinal cord injury in a male mouse model. *J. Neuroinflammation* **2022**, *19*, 134.

[47] Yang, T.; Dai, Y. J.; Chen, G.; Cui, S. S. Dissecting the dual role of the glial scar and scar-forming astrocytes in spinal cord injury. *Front. Cell Neurosci.* **2020**, *14*, 78.

[48] Wang, W. Z.; Sun, M. J.; Zhang, Z. D.; Guo, S.; Sun, H. J.; Wei, Z. J.; Ning, B. Application of microenvironment biomimetic materials in spinal cord injury and future prospects. *MedMat* **2025**, *2*, 137–139.

[49] Xia, Z. Q.; Zhang, J. H.; Ren, N.; Wang, S. P.; Zhang, C. C.; Malek, N. A. N. N.; Kamaruddin, W. H. A.; Liu, C.; Sun, C. H.; Wang, J. G. Neuronal differentiation and tissue engineering strategies for central neurous system injury repair. *BMEMat* **2025**, e70044.

[50] Shi, B. Q.; Lu, S.; Yang, H. R.; Mahmood, S.; Sun, C. H.; Malek, N. A. N. N.; Kamaruddin, W. H. A.; Saidin, S.; Zhang, C. C. One-dimensional nanomaterials for nerve tissue engineering to repair spinal cord injury. *BMEMat* **2025**, *3*, e12111.

[51] Liu, L.; Wang, W. T.; Huang, L.; Xian, Y. W.; Ma, W. Z.; Fan, J. H.; Li, Y. X.; Liu, H. M.; Zheng, Z. M.; Wu, D. C. Injectable pathological microenvironment-responsive anti-inflammatory hydrogels for ameliorating intervertebral disc degeneration. *Biomaterials* **2024**, *306*, 122509.

[52] He, S.; Li, Z. H.; Wang, L.; Yao, N. N.; Wen, H. D.; Yuan, H. G.; Zhang, J. T.; Li, Z. Q.; Shen, C. A. A nanoenzyme-modified hydrogel targets macrophage reprogramming-angiogenesis crosstalk to boost diabetic wound repair. *Bioact. Mater.* **2024**, *35*, 17–30.

[53] Gao, S. Q.; Yan, T. J.; Ji, L.; Pang, Y. D.; He, S.; Shen, C. A.; Wang, Z. M.; Zhang, J. T. Pathologically responsive Au@Ag nanocomposite spray-coated hydrogel dressing for accelerated healing of infected wounds. *ACS Appl. Mater. Interfaces* **2025**, *17*, 46693–46704.